





RESEARCH ARTICLE | SEPTEMBER 05 2023

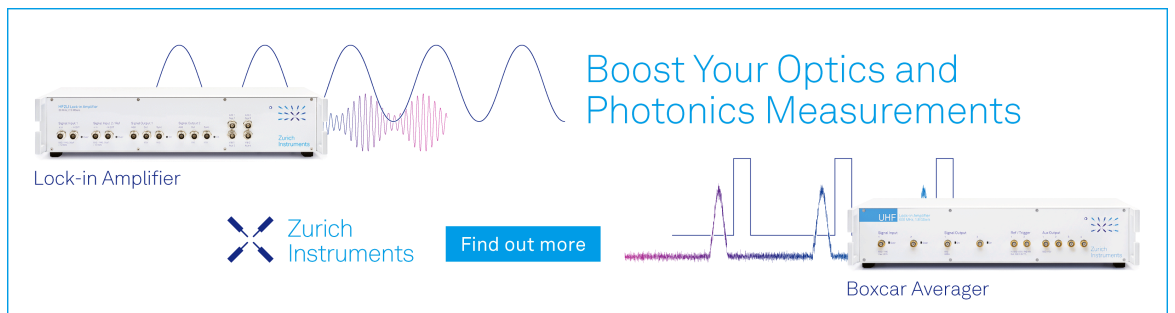
Understanding epitaxy of graphene: From experimental observation to density functional theory and machine learning

Ming-Sheng Zheng ; Shaojie Zhou ; Xinmo Wang; Lei Gao  




J. Appl. Phys. 134, 090901 (2023)

<https://doi.org/10.1063/5.0163580>



Boost Your Optics and Photonics Measurements

Lock-in Amplifier

 Zurich Instruments

[Find out more](#)

Boxcar Averager

Understanding epitaxy of graphene: From experimental observation to density functional theory and machine learning

Cite as: J. Appl. Phys. 134, 090901 (2023); doi: 10.1063/5.0163580

Submitted: 17 June 2023 · Accepted: 15 August 2023 ·

Published Online: 5 September 2023



Ming-Sheng Zheng,^{1,2} Shaojie Zhou,^{1,3} Xinmo Wang,^{1,2} and Lei Gao^{1,3,a)}

AFFILIATIONS

¹Beijing Advanced Innovation Center for Materials Genome Engineering, University of Science and Technology Beijing, Beijing 100083, China

²School of Chemistry and Biological Engineering, University of Science and Technology Beijing, Beijing 100083, China

³Corrosion and Protection Center, Institute for Advanced Materials and Technology, University of Science and Technology Beijing, Beijing 100083, China

^{a)}Author to whom correspondence should be addressed: gaolei@ustb.edu.cn

ABSTRACT

Due to enormous applications of large-area graphene with high quality, the epitaxial growth strategies have drawn a plethora of attention. However, the bottleneck in the production of graphene has caused delayed development in recent years, which is owing to the poor understanding of interaction mechanisms between graphene and the underlying metallic and non-metallic substrate. To understand the thermodynamics of graphene–substrate interface and growth kinetics, accurate density functional theory (DFT) calculations have been proved as an effective way, in terms of cost and time, compared with traditional experimental methods, which can calculate the interaction between graphene and substrates, helping us to better understand the practical phenomena. Here, we show the use of DFT methods to evaluate both van der Waals interaction and covalent bonding. Many of computational results fit well with the experimental observations. To address the relative low accuracy and small computation capacity (number of atoms) of common DFT models, we suggest that the machine learning (ML) methods will be a fresh impetus for epitaxial growth strategy of graphene, which put forward effective interpretations for complicated interconnections and correlations among the properties, thereby enabling ML a promising strategy for understanding, design, and synthesis of graphene over other 2D materials.

Published under an exclusive license by AIP Publishing. <https://doi.org/10.1063/5.0163580>

I. INTRODUCTION

Ideal two-dimensional (2D) material was thought to be an impossibility before the 21th century, since thermodynamic fluctuations at finite temperatures were believed to destroy the long-range ordering of atoms in any 2D crystals, leading to the decomposition or destruction of the crystal lattice.^{1,2} Thus, graphene was merely applied as a theoretical model for carbon materials, until Geim and Novoselov realized the successful exfoliation of single-layer graphene using the “scotch tape method,”³ and this discovery ushered in a new era of flat lands hosting exotic materials physics and superior physical properties.^{4,5}

Graphene, as a single atom thick 2D structure (0.33 nm), exhibits a crystal structure of the honeycomb lattice of sp^2 -hybridized

carbon atoms, which endows graphene with excellent electronic properties [the highest room-temperature (RT) carrier mobility],^{6–9} extraordinary high RT thermal conductivity (~ 5000 W/m K, much higher than diamond),¹⁰ remarkable mechanical strength (elastic modulus ~ 1 TPa and tensile strength ~ 130 GPa, 200 times stronger than steel).¹¹ Thus, graphene turns out to be a potential nanomaterial in battery electrodes, FET (field effect transistor) devices, thermal management, touch screens, gas sensors, medicine, and biology, etc.^{12–14} Combinations of excellent properties for graphene can be used in many applications listed above to replace the existing materials or realize the renovation of special equipment. However, one key difficulty to achieve the commercial production is how to prepare high-quality graphene in adequate quantities.

24 April 2024 17:19:13

Many preparation strategies of graphene have been developed up to now, which could be split into two different types including top-down “exfoliation” strategy and bottom-up “synthesis” strategy.¹⁵ The top-down “exfoliation” strategy is exfoliating graphene from the bulk graphite by a mechanical force, and the bottom-up “synthesis” strategy means growing graphene through carbon-precursor sources. In detail, the top-down “exfoliation” strategies mainly can be divided into mechanical and chemical exfoliation approaches. Actually, the “scotch tape method” is a kind of mechanical exfoliation methods using an adhesive tape to cleave the graphite layers apart.³ And other mechanical forces (e.g., sonication, micromechanical and grinding) are also effective measures for mechanical exfoliation. Although the straightforward procedure and low cost make this approach the most common method of fabricating graphene,^{16–19} and the introduction of highly oriented pyrolytic graphite (HOPG) promotes the further development in this field,^{20,21} the low yield, small size, uncontrollable layer numbers, impurities, and defects remain the main obstacles for practical applications. The chemical exfoliation approach is separating graphene from bulk graphite through a chemical process. Accurate selection of solvents turns out to be an important factor in this procedure. In addition, using acid, oxidizing agent, etc. (Brodie, Straudenmaier or Hummers methods) to prepare graphite oxide (GO),^{22–25} which exhibits much higher compatibility with solvent and makes it easier for a micromolecule insert into the layers of graphite oxide, enlarges the interlayer distance from 0.33 nm to 0.6–1.2 nm (thereby lowering the van der Waals force between layers). The effortless cleavage of GO due to weakened interlayer interaction attracted a great deal of attention for the reduced graphite oxide (rGO) method, and this kind of graphene is appropriate for nanocomposites, energy storage materials, and transparent electrodes. However, the fabrication of high-quality graphene in adequate quantities requires a special approach without damaging the crystals, which could be applied in electronic and semiconductor devices. The bottom-up “synthesis” strategies have the potential of preparing a single layer of graphene on the entire substrate. As the typical approach of bottom-up “synthesis” strategies, the epitaxial growth of graphene on a metal/nonmetal substrate turns out to be an attractive alternative to mechanical exfoliation.^{15,26} Epitaxial growth (e.g., chemical vapor deposition, temperature programmed growth, segregation) has been widely used to produce reactive carbon that binds to grow graphene through the high temperature (usually over 1000 °C) pyrolysis (during precipitation or on a surface). Remarkable progress has been achieved in this direction, using both metals and inorganic nonmetals as the substrate.^{27,28} The metal or nonmetal surface not only plays a catalytic role in the dissociation and recombination of the precursor, but also acts as a growth template during the process of graphene growth. Graphene can grow on different substrates because of the peculiarities of preparation techniques.^{29,30} Due to the unclear mechanism of the role of substrates and their effect on electronic transport in graphene, many experimental and theoretical studies have been carried out to reveal the inherent relation and regularity of the epitaxial growth of large-area graphene with quantity production.

In this work, structural properties of graphene on a number of close-packed metals (e.g., Pt,³¹ Ir,³² Cu,³³ Ru,³⁴ Fe,³⁵ Ni³⁶) and

non-metal (SiC,³⁷ mica,³⁸ Al₂O₃,³⁹ SiO₂⁴⁰) surfaces will be discussed.⁴¹ After that, some of the existing simulation techniques were analyzed, especially the density functional theory (DFT), which have been proven extremely useful in understanding graphene growth.^{42–44} However, there are two main obstacles need to solve. First, a more accurate method is urgently required to calculate the complex interactions between the graphene and substrates. Second, DFT for graphene growth needs an effective approach to overcome the size limitation of calculation, and machine learning (ML) method is considered as the most promising way to address this issue.^{45–47} In light of the two obstacles, the experimental results, the interaction calculation methods (DFT especially) and machine learning algorithms will be discussed in detail.

II. EXPERIMENTAL PROGRESS OF GRAPHENE GROWTH ON METALLIC AND NON-METALLIC SUBSTRATES

A. Interaction between graphene and metallic substrates

Graphene grown on metallic surfaces has resulted in various properties due to the lattice mismatch between graphene and substrate.⁴⁸ This translates into a superior stiffness of graphene. Biaxial strain in graphene, which may arise from epitaxial stress during graphene growth on a substrate, is consequently especially energetically costly.⁴⁹ Actually, the epitaxial structure, height, and flatness of graphene on metal surfaces are determined by both the interaction strength (e.g., covalent bond and van der Waals interaction) and lattice matching between two-dimensional atomic crystal and metallic substrates.⁵⁰ A series of noble metallic or transition metallic surfaces have also been demonstrated to have catalytic activity in low pressure and high vacuum environments and can be used as substrates in the preparation process of graphene. Metallic substrates that have had graphene grown on them successfully include Pt, Ir, Cu, Ru, Ni, and Fe, etc., which could be divided as substrates with weak and strong interaction and will be discussed, respectively.

1. Metallic substrates with weak interaction

Due to the weak interactions between substrate and graphene,^{51,52} graphene grown on the metallic surface, such as Pt, Ir, Cu, etc., usually shows flat shape, but polycrystalline structures with multi-lattice orientation. And, the weak binding energy caused by weak interaction also plays an important role in the growth mechanisms, structure, and electronic properties of graphene, which are distinct from the graphene growth on the metals with strong interaction.

Pt is more resistant to oxidation than the widely used easily oxidized metals (e.g., Ni and Cu due to its remarkable inertness),⁵³ with an excellent catalytic ability for subsequent graphitization and decomposition of hydrocarbons,⁵⁴ Pt can induce growth of large-grain graphene at ambient pressure, which lowers the harsh preparation conditions of graphene growth.⁵⁵ Due to the relatively weak interaction between graphene and Pt(111) surface,⁵⁶ many rotational domains could be observed in the graphene growth on the Pt(111) surface.^{57,58} As shown in Figs. 1(a) and 1(b), Sutter *et al.* used low-energy electron microscopy (LEEM) to detect the

24 April 2024 17:19:13

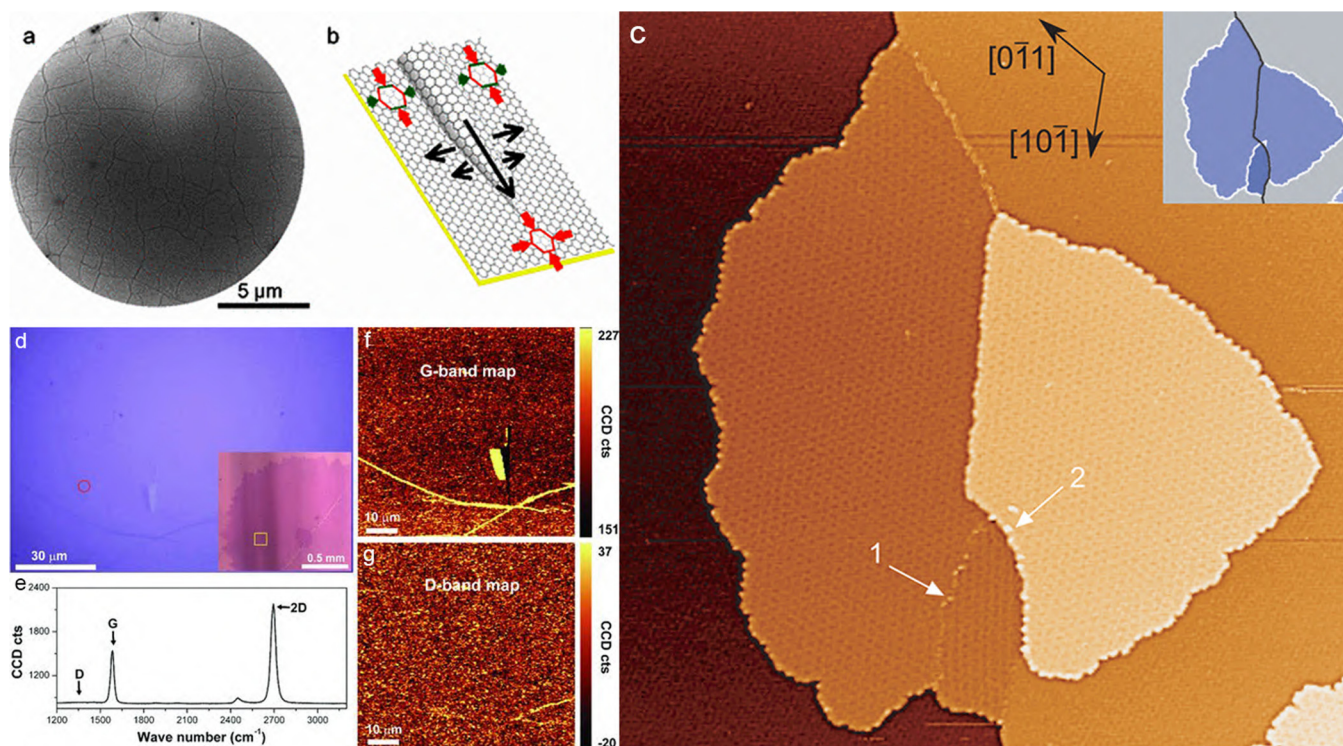


FIG. 1. (a) LEEM and (b) schematic image of graphene on Pt(111). Reproduced with permission from Sutter *et al.*, Phys. Rev. B **80**, 245411 (2009). Copyright 2009 American Physical Society. (c) STM topography of graphene on a Ir(111) surface. Reproduced with permission from Coraux *et al.*, New J. Phys. **11**, 023006 (2009). Copyright 2009 IOP Publishing. (d)–(g) Optical micrograph and Raman results of graphene on the Cu foil. Reproduced with permission from Chen *et al.*, Adv. Mater. **25**, 2062 (2013). Copyright 2013 Wiley.

24 April 2024 17:19:13

characteristic of the graphene growth process with a weak metal-graphene interaction, which clearly showed the wrinkle in practical and schematic images,⁵⁹ and barely different growth rates across substrate steps were observed.

It is well known that weak interaction between Ir and graphene is beneficial for the accurate control on the electronic band structure of graphene.⁶⁰ In addition, the low C solubility in Ir is favorable for the achievement of high-quality graphene.⁶¹ Coraux and co-workers grew graphene on Ir(111) foils through two growth methods including temperature programmed growth (TPG) at 870–1470 K and chemical vapor deposition (CVD) at 870–1320 K.⁶² Compact graphene islands bounded by C zigzag edges were detected in the process of TPG as shown in Fig. 1(c), and their sizes could be regulated from several to dozens of nanometers through Smoluchowski ripening. In addition, the decomposed carbon atoms from ethene molecules on the Ir(111) surface showed extremely high conversion rate to graphene in the procedure of CVD.

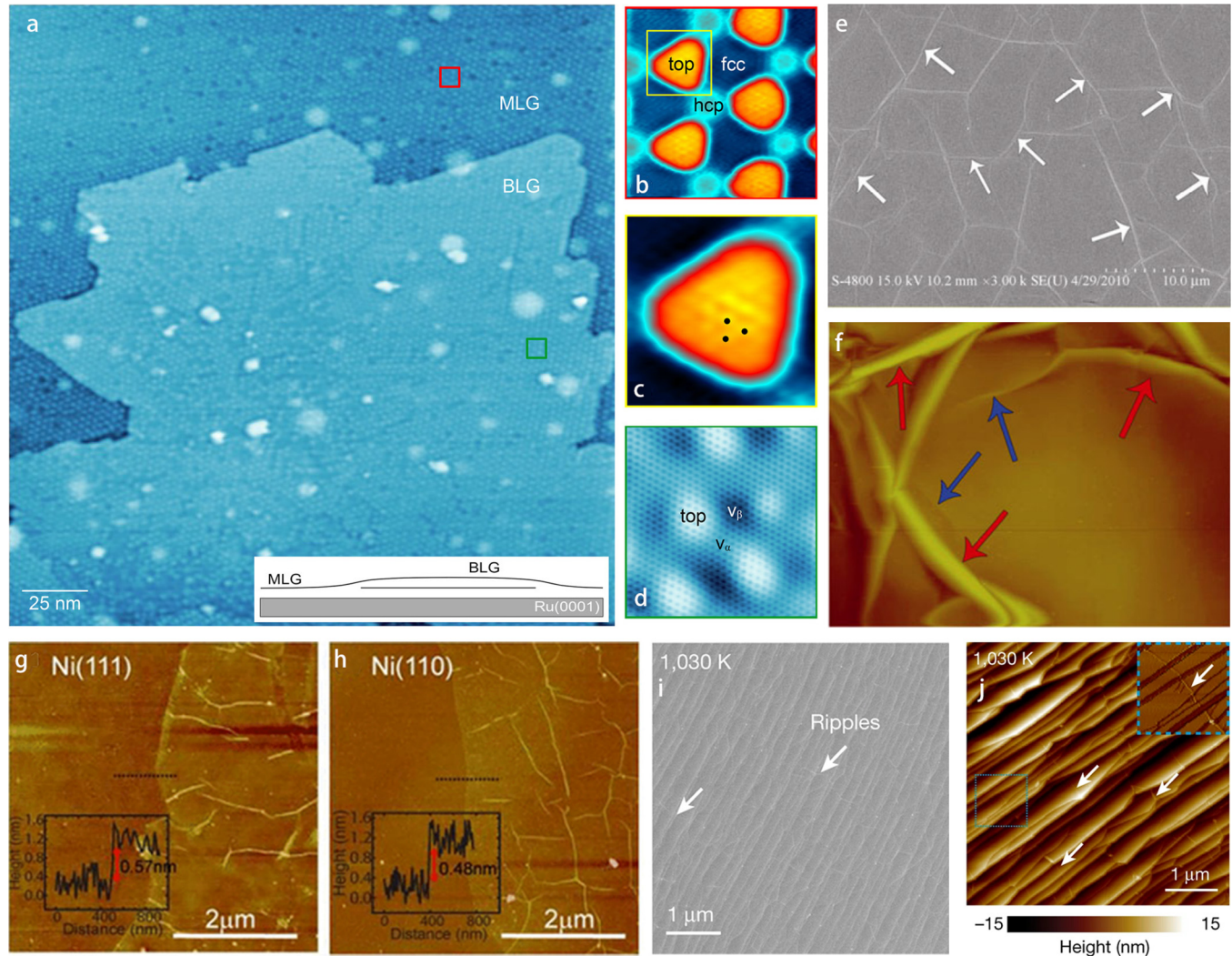
Cu not only has the proper in-plane lattice parameter, but also shows much low carbon solubility (7.4 at. ppm at 1020 °C) and carbon diffusion rate,^{63,64} which is beneficial for studying the phenomenon of graphene growth by the CVD method and has been used for the production of graphene in the industry.⁶⁵ Moreover, due to the relatively low melting point of Cu (1385 K),

the mobility of C atoms on the surface of Cu substrate is greatly stronger than the Ni substrate, and the released heat during the formation of C–C bond causes a molten status on the surface of the Cu substrate, leading to a disordered state of Cu atoms on the surface.⁶⁶ In addition, due to the phase transition (molten status) on the surface of the Cu substrate, the enhanced mobility of Cu atoms on the surface of the substrate will significantly promote the defect self-healing of graphene, which also promote the higher quality of graphene grown on the Cu(111) surface as shown in Figs. 1(d)–1(g).

2. Metallic substrates with strong interaction

On the substrates (e.g., Ru, Fe, Ni) that interact strongly with graphene, graphene can easily form a single-crystal structure, however periodic morphological corrugation (moiré structure) is also observed.⁶⁷ Although the presence of the moiré pattern locally changes the electronic structure of the graphene overlayer,⁶⁸ the remarkable graphene/metal system with a moiré pattern has been thought as an ideal template for self-assembled nanostructures.^{69,70}

The interaction between Ru and C atoms enables the growth of graphene on the Ru(0001) surface, so single-layer graphene on Ru is a typical example of the strong-coupling limit.⁷¹ And, a

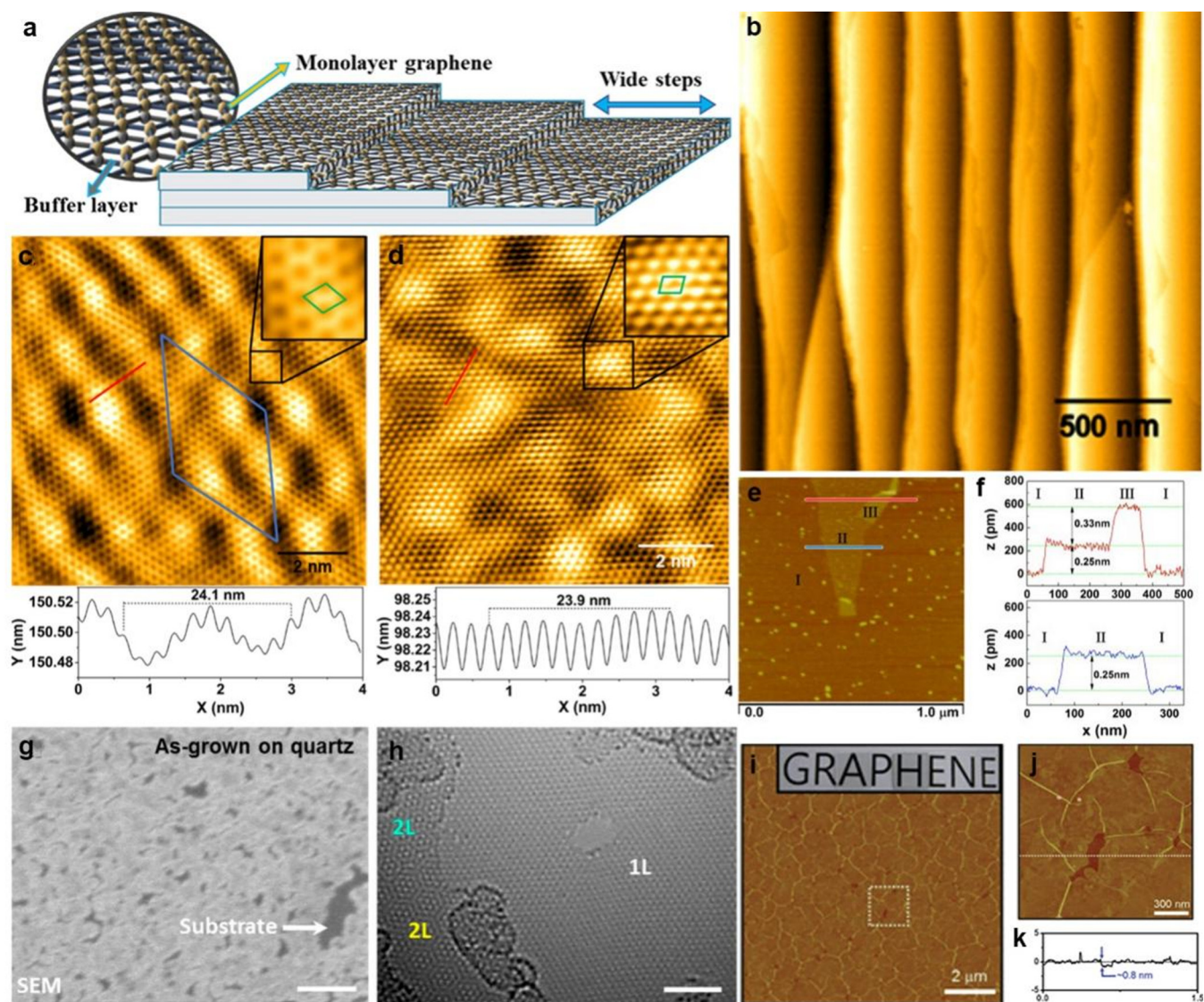


24 April 2024 17:19:13

FIG. 2. (a) Graphene and (b)–(d) its moiré pattern on Ru(0001). Reproduced with permission from Halle *et al.*, *J. Phys. Chem. Lett.* **12**, 6889 (2021). Copyright 2021 ACS Publications. (e) SEM and (f) its AFM images of graphene on Fe foils. Reproduced with permission from Xue *et al.*, *Nano Res.* **4**, 1208 (2011). Copyright 2011 Springer. AFM images of graphenes transferred to Si-SiO₂ for graphenes grown on the surface of (g) Ni(111) and (h) Ni(110). Reproduced with permission from Mafra *et al.*, *Phys. Rev. Mater.* **2**, 073404 (2018). Copyright 2018 American Physical Society. (i) SEM and (j) AFM images of graphene on Cu-Ni(111) alloy foils. Reproduced with permission from Wang *et al.*, *Nature* **596**, 519 (2021). Copyright 2021 Springer.

moiré pattern can be observed because of the lattice mismatch between graphene and Ru (the moiré hexagonal lattice has a period of around 30 Å),^{71,72} as shown in Figs. 2(a)–2(d). In addition, the strong interaction is the main factor of producing corrugation in the Ru substrate, and the peak to peak height about 1.5 Å⁷³ of these corrugations have been measured using low-energy electron diffraction (LEED). It is well known that carbon precursor on the metal surface originated from the dissociation of feedstock gas plays an important role in the controllable growth of graphene. Thus, the state of graphene growth on Ru(0001) could be regulated by the supersaturated 2D gas of C adatoms.⁷⁴

From a practical point of view, the idea of fabricating graphene on the surface of iron (Fe) has attracted much attention because of the low cost in comparison with using other transition metal substrates and availability of easy etching methods. It has been found that the a face-centered cubic γ -austenite with the maximum solubility of carbon ~ 2.14 wt. % is obtained in the Fe–C mixture at a temperature range between 1147 and 912 °C, while a phase transformation to body-centered cubic α -ferrite could be observed, leading to a reduced solubility of C, then lowering the temperature to 727 °C caused the formation of eutectic phase with a solubility as low as 0.022 wt. %.⁷⁵ The transformation from high temperatures to



24 April 2024 17:19:13

FIG. 3. (a) The model, (b) AFM topography, (c) and (d) STM images of the moiré structure for graphene on the SiC steps. Reproduced with permission from Zebardastan *et al.*, *Nanotechnology* **34**, 105601 (2022). Copyright 2022 IOP Publishing. (e) AFM image and (f) step height scans of graphene on the mica substrate. Reproduced with permission from Lippert *et al.*, *Carbon* **52**, 40 (2013). Copyright 2013 Elsevier. (g) SEM image and (h) HRTEM image of graphene on the quartz glass surface. Reproduced with permission from Sun *et al.*, *Nano Lett.* **15**, 5846 (2015). Copyright 2015 ACS Publications. (i) AFM, (j) HRAFM images, and (k) step height scans of graphene on the α -Al₂O₃ surface. Reproduced with permission from Song *et al.*, *Nanoscale* **4**, 3050 (2012). Copyright 2012 Royal Society of Chemistry.

low temperatures was beneficial for the growth of few-layered graphene films, as shown in Figs. 2(e) and 2(f). As a result, the size of the iron foil determined the area of the graphene films, which is only restricted by the size of the CVD chamber. More importantly, the complex Fe-C phase diagram also offers versatility at different phase stages for engineering graphene layer numbers.^{76,77}

It has been well known that the nearest neighbor atomic spacing of the Ni (111) crystal is 2.49 Å, which is almost the same as the in-plane lattice parameter of graphene (2.46 Å), resulting in

high lattice compatibility.^{78,79} The growth of the 2D atomic crystal surface structure of graphene on the surface of the metal with higher lattice matching degree causes less moiré pattern and higher flatness. Therefore, the synthesis of high quality and large-scale graphene on the Ni(111) surface is reliable, which will also promote the preparation of graphene with fewer defects. Mafra and her co-workers grew large-area single-layer graphene through ambient pressure chemical vapor deposition on the surfaces of Ni(111), Ni(110), and Ni(100), respectively.⁸⁰ Figures 2(g) and 2(h) show the

single-layer graphene on the order of a few cm^2 grown on Ni(111) and Ni(110), respectively. Even on the surface of Ni(100), for which it was thought organized carbon structures were unlikely or not possible to exist, it was found that grew multilayer graphene, showing an surprising benefit for different technological applications.

The higher catalytic activity of Ni enhances the growth rate of graphene significantly; however, the remarkably large carbon solubility results in poor control of the dissolved C atoms, which mainly leads to nonuniform multilayer graphene. In contrast, the extremely low carbon solubility and self-limited growth on Cu improve the growth of single-layer graphene, but the low catalytic activity also brings slowed growth rate. Thus, the idea of combining the advantages of both Ni and Cu was proposed to simultaneously achieve the goal of synthesizing large-area single-crystalline graphene with fast growth rate and low nucleation density.⁸¹ For example, Wang *et al.* reported that a large-area, fold-free, single-layer graphene film was fabricated successfully on single-crystal $\text{Cu}_{80}\text{Ni}_{20}$ alloy foils in a growth temperature range of 1000–1030 K using ethylene as the carbon precursor,⁸² which showed an average room-temperature carrier mobility of around $7.0 \times 10^3 \text{ cm}^2 \text{ V}^{-1} \text{ s}^{-1}$ for both holes and electrons. The results demonstrated that the interfacial compressive stress originated from the shrinkage of the Cu–Ni(111) foil substrate at the growth temperature down to 1030 K prompted the formation of graphene perpendicular to the step edge direction, thus large-area, single-layered graphene with high-quality and fold-free were prepared, as shown in Figs. 2(i) and 2(j).

There are many other types of metallic catalysts such as Rh, Re, Au, etc., which also exhibit attracting properties of growing graphene. For example, due to the interaction strength of Rh between the surface and graphene lies in between Ru and Ir, graphene grown on the Rh(111) foil has a similar structure with that on Ru (0001), so does Re.⁸³ In particular, Nie and co-workers studied the performances of graphene islands on the surface of Au(111) fabricated through deposition of elemental carbon at 950 °C and found that the most of graphene islands exhibited dendritic shapes, which was inclined to cover valleys on the surface of gold foil, suggesting that Au was displaced as the graphene grew.⁸⁴ According to all of the metallic catalysts discussed above, the interaction as well as the lattice matching between metal and C atoms is essential for the growth performances of graphene. Thus, choosing a proper lattice structure and exploring the interaction mechanism are beneficial for the production of high-quality graphene in adequate quantities.

B. Interaction between graphene and non-metallic substrates

Many metals (especially transition metals) have been proved as powerful catalysts. However, an additional technology for mechanical transfer of graphene from the surface of metal to non-metallic substrates is needed, especially for electronic applications.⁸⁵ Thus, the epitaxial growth on the non-metallic surfaces is also a potentially useful way to prepare large-area single-layer graphene, since no transfer is needed in this case. In addition, when graphene is used as an intermediate layer between the substrate and growth material in the remote epitaxy procedure, which is also an important method to prepare other kinds of 2D materials, the

electrostatic potential of the substrate below graphene can affect the growth material at the range of several Å.

1. Epitaxial growth of graphene on the non-metallic substrate

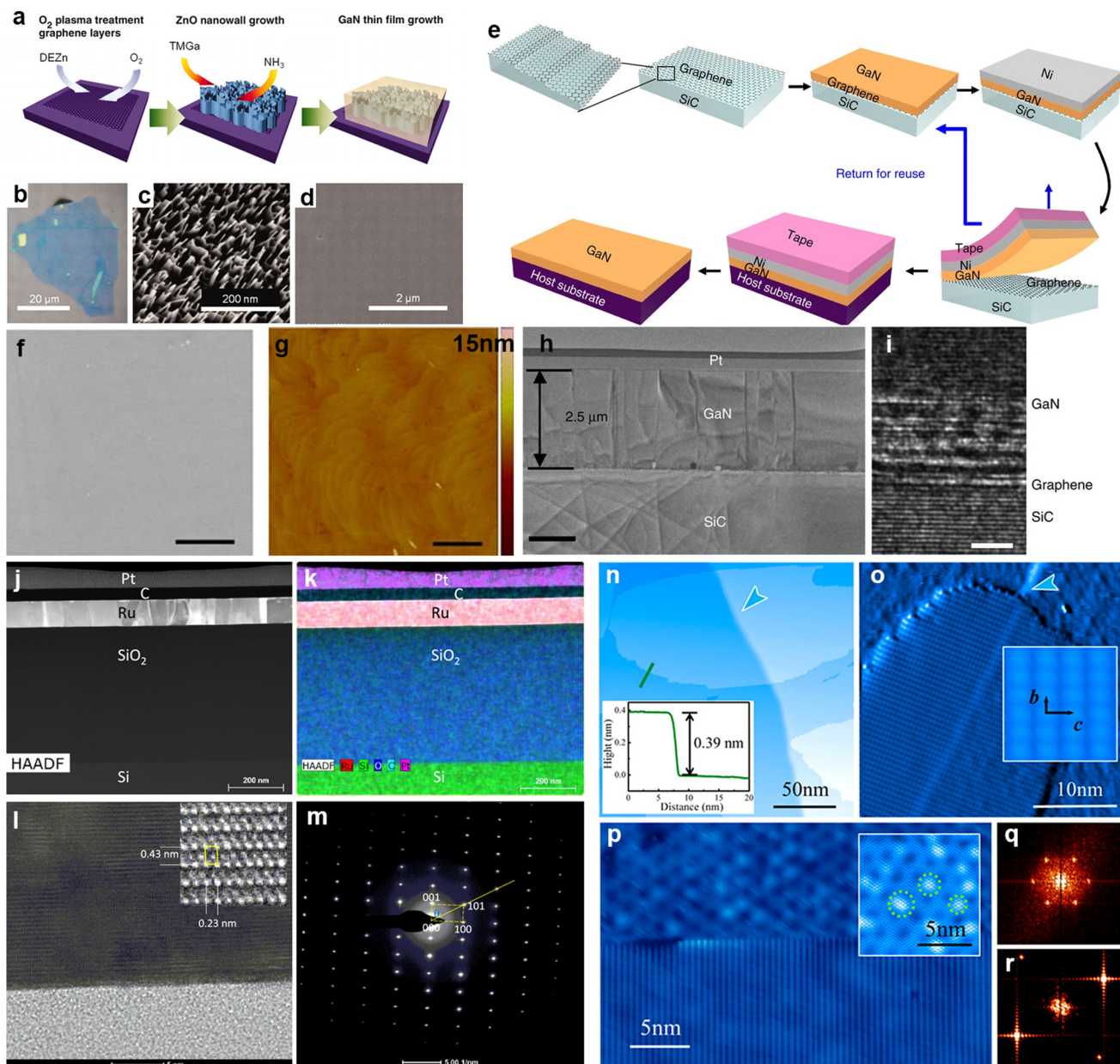
Silicon carbide (SiC) is a superior semiconductor insulating substrate material, and the epitaxial growth of graphene on SiC substrates has been considered to be the most promising and compatible method with existing semiconductor process technologies and the preparation of graphene-based electrical devices.⁸⁶ Through heating SiC single crystals at high temperatures, the Si atoms on the SiC surface are evaporated and the remaining C atoms self-assemble to form graphene. However, this SiC-based epitaxial graphene method has complex kinetic and thermodynamic processes, including the sublimation and precipitation of Si atoms on the substrate as well as the nucleation, diffusion, and growth of C atoms, etc.⁸⁷ Zebardastan *et al.* reported the face-to-face annealing of SiC in ultra-high vacuum recently, which could grow virtually defect-free single graphene layers and cover the SiC steps [Fig. 3(a)]. As shown in Fig. 3(b), the optimized growth condition led to high-quality graphene (1.9 layers) and terrace width (above 440 nm), and the moiré structure was also observed in Figs. 3(c) and 3(d).⁸⁸

Lui *et al.* found the deposition of graphene onto the surface of mica could produce ultra-flat graphene in 2009, which was helpful for rigorous testing of the influence of ripples on various properties of graphene.⁸⁹ Lippert found that the direct growth of graphene could be realized by molecular beam epitaxy (MBE) of C atoms on the surface of muscovite mica (a kind of van der Waals substrate).⁸⁵ Further work of Lippert revealed that it indeed has a processing window for the growth of graphene with high quality, because small graphene spots can freely slide over the flat surface regions, collecting C atoms reacted with the surface, and fetch O atoms to sites reduced by C atoms.⁹⁰ They used biotite mica as the substrate, which exhibits better thermal stability than muscovite mica, and the single-layer graphene grown directly on mica surface with high crystalline quality and the size in the micrometer regime was obtained, as shown in Figs. 3(e) and 3(f).

Complicated post-growth techniques of graphene sheets are necessary to transfer them onto the dielectric substrate (SiO_2 or Si) for the use of graphene in practical electronic devices, which also leads to material wastage. Thus, if direct graphene growth onto the desired dielectric substrate was realized, unnecessary post-growth processing and material wastage could be avoided. Sun *et al.* reported an atmospheric-pressure chemical vapor deposition (APCVD) approach to realize direct well-controlled growth of high-quality graphene on solid glass (its main components is SiO_2) at 1000–1100 °C,⁹¹ as shown in Figs. 3(g) and 3(h). The sheet resistance and optical transparency of the graphene/glass system can be manipulated together with the layer thickness of graphene.

Due to high melting point (>2000 °C), the hexagonal symmetry and the possibility of lattice-matched epitaxial growth, sapphire (main component is Al_2O_3) was also applied as the substrate for growing graphene without any other catalyst. Song and co-workers prepared a large-area and high yield single-layer graphene film using a transparent sapphire ($\alpha\text{-Al}_2\text{O}_3$) as the substrate through a

24 April 2024 17:19:13



24 April 2024 17:19:13

FIG. 4. (a) Schematic illustrations, (b) optical microscopic image and (c) and (d) SEM images of the GaN thin film grown on ZnO nanowalls on graphene. Reproduced with permission from Chung *et al.*, *Science* **330**, 655 (2010). Copyright 2021 The American Association for the Advancement of Science. (e) Schematic, (f) SEM, (g) AFM and (h) and (i) TEM images of growing single-crystalline GaN films on epitaxial graphene. Reproduced with permission from Kim *et al.*, *Nat. Commun.* **5**, 4836 (2014). Copyright 2014 Springer. (j)–(m) TEM images of a 94.2 nm thick Ru film on the surface of the graphene/SiO₂ substrate.⁹⁹ Reproduced with permission from Lu *et al.*, *ACS Appl. Electron. Mater.* **4**, 5775 (2022). Copyright 2022 ACS Publications. (n)–(r) Topographic images (STM) of Te films on graphene. Reproduced with permission from Huang *et al.*, *Nano Lett.* **17**, 4619 (2017). Copyright 2017 ACS Publications.

CVD process at 950 °C,⁹² which exhibited the characteristics of a Dirac point. The large-scale [up to 2 in. α-Al₂O₃ (0001) wafer] was obtained in Figs. 3(i)–3(k), which has enormous potential of transfer-free fabrication of top-gated FETs. By designing an

electromagnetic induction heating CVD operated at elevated temperatures, Chen *et al.* found that the problems of high pyrolysis and migration barriers of C atoms could be solved, leading to a wafer-scale highly oriented graphene growth on the surface of

sapphire.⁹³ Moreover, γ -Al₂O₃ was also applied as a substrate for the highly efficient growth of graphene by Park,⁹⁴ which allowed the preparation of graphene/dielectric layer structures and even grain size customization.

2. Epitaxy of materials through the graphene coated substrate

Since the discovery of graphene, the growth of additional materials (films) on top of graphene to obtain flexible devices is not only the frontier of materials science research, but also has practical value for a variety of devices. More importantly, due to the unique properties of graphene, it provides a feasible solution for obtaining low-cost, large-size, high-quality films. Epitaxial film growth generally requires the same or similar lattice structure and small lattice mismatch between the substrate and the film. However, the lattice of epitaxial films is usually significantly different from that of the substrate, which will affect the quality of the film. For van der Waals epitaxial growth strategy, the weak van der Waals forces between substrate and epitaxial layer can greatly reduce the requirement of lattice matching, and the absence of covalent bonds between layers will further unlock the restrictions of types of prepared materials.⁹⁵

Chung *et al.* realized van der Waals epitaxy of group III nitrides based on mechanically exfoliated graphene for the first time in 2010. Epitaxial high-quality GaN films was grown on the oxygen (O₂) plasma-treated graphene/sapphire substrates by using densely and vertically aligned zinc oxide (ZnO) nanowalls as the interlayer [Figs. 4(a)–4(d)].⁹⁶ More importantly, because of the weak van der Waals interactions between graphene and nitride epilayer, the GaN films can be easily transferred to other target substrates through physical methods. Kim grew high-quality single-crystal GaN films on SiC epitaxial graphene through van der Waals epitaxy,⁹⁷ as shown in Figs. 4(e)–4(i), and its average dislocation density about 10⁹ cm⁻² and RMS surface roughness of 3 Å were comparable to those of thin films grown on sapphire or conventional SiC substrate. In addition, by combining homoepitaxial growth of GaAs(001) on the single-layer graphene/GaAs(001) substrate with DFT calculations, they further demonstrated that adatoms experienced remote epitaxial registry through a substrate–epilayer gap (~9 Å) with a substrate, which could accommodate a single-layer graphene.⁹⁸ And, this result proves that the application of graphene in the remote epitaxy is an effective way toward defect-free hetero-integration of dissimilar materials and cost saving.

In addition, single-element thin films were also available for the epitaxy strategy through graphene coated substrate. Lu *et al.* fabricated an epitaxial Ru ultrathin film on graphene through the quasi van der Waals epitaxy approach using magnetron sputtering at 600 °C. As shown in Figs. 4(j)–4(m), the film with a thickness ranging from 3.9 to 94.2 nm was obtained, which showed excellent electrical property.⁹⁹ Tellurium (Te) films with monolayer and few-layer thickness were also prepared by Huang *et al.* through molecular beam epitaxy on a graphene/6H-SiC(0001) substrate.¹⁰⁰ It was found that the bandgap of Te rose monotonically with the reducing thickness, and the value of the monolayer Te reached 0.92 eV. The film with the bulk-truncated (1 × 1) structure was also obtained [Figs. 4(n)–4(r)].

III. SOLUTIONS BASED ON CALCULATION METHODS

According to the discussion of the experimental developments for epitaxial graphene growth, preparing high-quality graphene with various functions are still needed to meet the requirement of innovating numerous materials and devices as expected. And the preparation of graphene requires systematic and rapid exploration on the current basis, but traditional trial-and-error experimental methods are costly and time-consuming, and computing has great potential to rapidly advance the experimental process in this regard. The DFT method can calculate the interaction between graphene and substrates, thus helping us to better understand the experimental phenomena. How to calculate the accurate long-range interaction is the key to the validity of the calculation. Grimme method,^{101,102} vdW method,^{103,104} etc., can be used to describe the morphology and properties of graphene on a 3D substrate more accurately. And, machine learning is good at enlarging the calculated quantity and realizing precise prediction after effective training, which has been proved in many other fields. Thus, choosing proper computing methods is beneficial for the further development of epitaxial growth of targeted graphenes.

A. DFT method to calculate graphene/metal interaction

1. Calculations involving metallic substrates with weak interaction

Gao *et al.* studied the influence of growth temperature and ethylene exposure in the epitaxial growth of graphene on the Pt(111) surface.¹⁰⁵ Two structural models were built and calculated by DFT calculations to investigate the geometric and electronic structures. The calculated average adhesive energies of per C atom are 38.6 meV [8 × 8 graphene unit cells on 7 × 7 unit cells of Pt(111)] and 39.8 meV (2 × 2 supercell) for the two models, which demonstrated the small interaction between graphene and the Pt(111) surface, and an interfacial distance of more than 0.31 nm was also obtained indicating the weak graphene–substrate interaction.¹⁰⁶ Kim and co-workers investigated the growth of graphene on the surface of Pt(111) in stages at different annealing temperature of the precursor hydrocarbon decomposition.¹⁰⁷ DFT calculations with Vienna *ab initio* simulation package (VASP) employing the generalized gradient approximation functional with the Perdew–Burke–Ernzerhof (PBE) form and project-augmented wave (PAW) method was carried out,^{108,109} which confirmed the figuration of dome-shaped graphene and the structural transformation from a smaller dome-shaped to larger basin-shaped graphene. The extracted atom positions and corresponding strain were introduced to calculate the pseudo-magnetic field, and the results demonstrated that the electronic structures of graphene were affected due to the electron confinement promoted by the nanoscale-size effect. The structural changes were also found to have a significant effect on the electronic properties. Kang *et al.* proposed that using twinned Pt (111) films as the substrates could grow 6-in. single-crystal graphene by ambient-pressure CVD, which showed quick growth rate and ultrahigh thermo-stability even under high-temperature air conditions (>500 °C).¹¹⁰ As a typical model during the initial growth, C₂₄ cluster was performed to investigate the

24 April 2024 17:19:13

inherent mechanism of uniform formation of graphene domains on the twinned Pt surface, as shown in Figs. 5(a)–5(d), and through the calculations of energy barrier, it was found that the energy barrier can be completely eliminated due to chemical potential difference between the carbon feedstocks and graphene was over 0.5 eV, meaning that the graphene growth is not significantly limited by the formation of a 60°-twin structure of Pt(111), which was the main reason of the highly qualified growth of graphene on the twinned Pt (111) surface.

Coraux and co-workers found that the modified Langmuir adsorption model fit well the measured coverages for the growth of graphene on the Ir(111) foil by the CVD method at 1120 K,⁶² indicating no desorption occurred. However, the simple Langmuir adsorption model is not suitable for many other situations. Six types of moiré superstructures of graphene on Ir(111) with different orientations are investigated combining experimental and computational data. The different geometric environment as well as electronic structures of C atoms for all the observed moiré patterns were revealed by DFT based first-principles calculations involving van der Waals interaction. And, the results demonstrated that the weak interaction between graphene and the Ir(111) substrate caused the coexistence of multi-oriented moiré superstructures. In addition, because of interactions with the substrate, graphene nanoislands on metal substrates have been thought as no existence of edge states.¹¹¹ Chen *et al.* demonstrated that intercalating a layer of Si atoms between the graphene nanoislands and the substrate could recover the edge states of graphene nanoislands on an Ir surface.¹¹² The DFT calculations performed using VASP indicated that the buffer layer of Si could effectively suppress the interaction between the graphene and Ir, and the edge states gradually shifted to the Fermi level with increasing lateral sizes of the GNIs, as shown in Figs. 5(j) and 5(k), which fits well with the experimental results shown in Figs. 5(e)–5(i).

Unlike other popular catalysts (e.g., Pt, Ir, Ni), Cu is usually in a surface molten state in the graphene growth procedure without subsurface diffusion of carbon, which needs a special model to simulate the growing process. The quantum chemical molecular dynamics (QM/MD) simulations [a four-layer Cu model including a 6 × 6 slab (144 atoms in total)] were performed to discuss graphene growth on the Cu(111) surface.¹¹³ And, the second-order density functional tight-binding (SCC-DFTB) method for the investigation of graphene nucleation on Cu(111) at 1180 K revealed the mechanism of defect healing and graphene growth, which proposed that defects at the edge of the growing graphene could be removed quickly due to the highly diffusive Cu atoms at high temperatures. Li *et al.* revealed that the epitaxial graphene grown on the surface of Cu(111) was wrinkle free and its biaxial compressive strain was at the range from 0.15% to 0.50%.¹¹⁴ In this work, DFT calculations implemented in the VASP were introduced to simulate the total energy of graphene sliding on the Cu (111) surface.¹¹⁵ The interactions between electrons and ions were described by the PBE functional and PAW pseudopotential, and the DFT-D3 method was used to correct the weak van der Waals interaction between graphene and the Cu (111) surface. The results demonstrated that the transition from flat graphene to graphene with a wrinkle depends on the van der Waals binding between graphene layers, the bending stiffness of graphene, the adhesion of the graphene to

the substrate and the friction force of graphene sliding on the substrate, as shown in Figs. 5(l)–5(q). Furthermore, the frictional forces in both epitaxial and non-epitaxial graphene were estimated through the first-principles calculations. Due to the total energy of epitaxial graphene between 2 and 4.5 meV per atom [Figs. 5(p) and 5(r)], the frictional force was estimated to be in the range from 9.6×10^7 to 2.2×10^8 N m⁻², which was about two orders of magnitude higher than that of the non-epitaxial graphene, indicating the scarce formation of wrinkles for epitaxial graphene although the compressive strain is higher (0.25%–0.40%), shown in Figs. 5(m) and 5(n).

2. Calculations involving metallic substrates with strong interaction

As shown in Figs. 2(b)–2(d), a hexagonal structure with a periodicity about 3 nm was assigned to a moiré pattern. Wang *et al.* designed a supercell (consisting of 651 atoms) on three-layer slab of Ru atoms including an (11 × 11) lateral periodicity and one layer of (12 × 12) graphene.⁷² The VASP package based on DFT implemented plane waves and PAW pseudopotentials was performed to describe the electron/ion interaction. It was demonstrated for the first time that the interaction between Ru and graphene consisted of not only the van der Waals binding but also a strong C–Ru bond origin from orbital hybridization between the Ru and graphene. Thus, Ru is a metallic substrate with strong interaction, also including Fe, Ni, etc.

Silva *et al.* carried out further research on the interaction between graphene and Ru(0001).¹¹⁶ In conjunction with DFT calculations using a remarkably large unit cell [an extended slab model of six (23 × 23) Ru layers, and a (25 × 25) C layer (4424 atoms)] and non-local interactions, good agreement between the experimental data and the DFT calculations was observed on not only the chemisorbed graphene at valleys, but also the weakly interacting graphene at hills. And the results also resolved the uncertain factors in the work reported by Moritz *et al.*^{73,117} DFT with the PAW method implemented in the VASP was performed to investigate the morphology and of microstructure graphene on the Ru (0001) surface with different rotation angles by Gao and co-workers, using the optB86b-vdW exchange correlation functional to approximately describe the van der Waals interaction.¹¹⁸ The results indicated that the moiré superlattice periodicity, graphene corrugation, as well as the interaction energy between graphene and Ru(0001) were suppressed as a function of the rotation angle. Zhu and Ding applied the first-principles calculations using VASP and van der Waals correction method (DFT-D3) to estimate the sizes and the morphologies of highly stable graphene quantum dots.¹¹⁹ The vertical distance between the Ru(0001) surface and graphene periodically vibrated between 2.19 and 3.50 Å, and a moiré pattern with a periodicity of 2.95 nm was also observed, as shown in Figs. 6(a)–6(f). They found that both the moiré structure-modulated interaction (the main factor) of graphene edge–metal substrate and the oscillation (the secondary factor) determined the sizes and shapes of graphene, as shown in Fig. 6(g), which fits well with the experimental results of Ref. 120.

The advantages of Fe as the substrate, such as low cost and availability of easy etching methods, have attracted much attention

24 April 2024 17:19:13

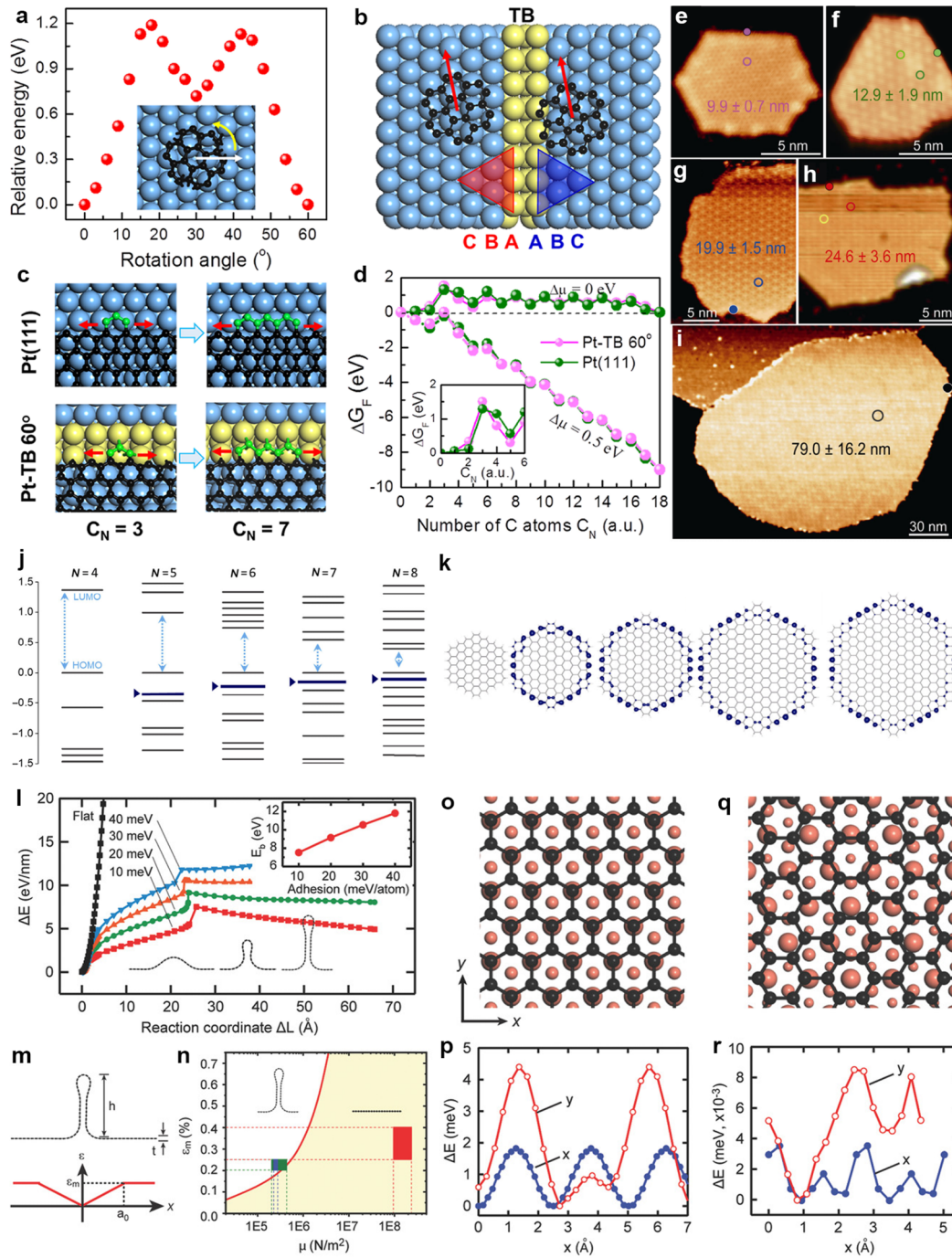
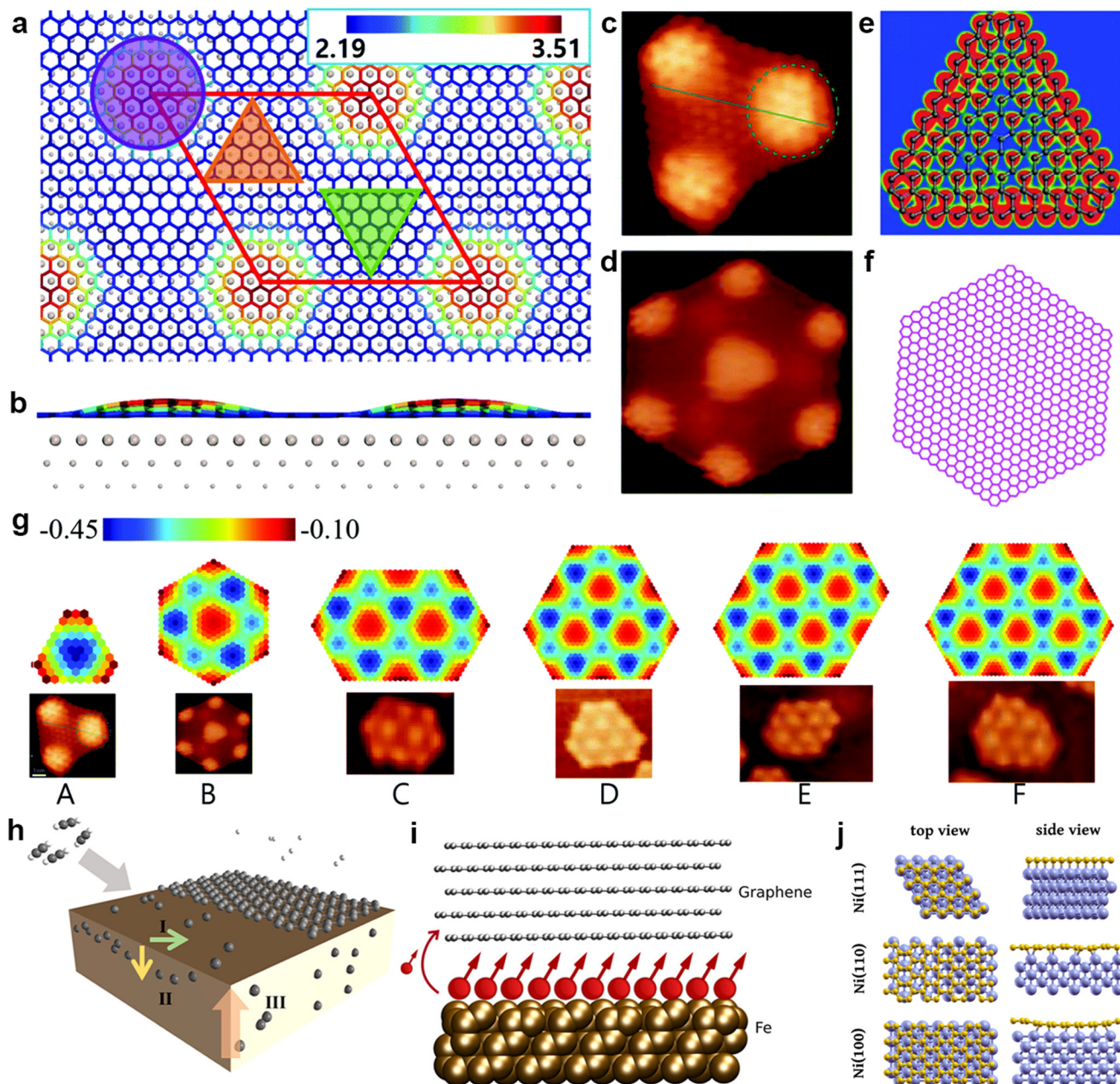


FIG. 5. (a)–(d) The investigation of the inherent mechanism of graphene domains on the Pt surface during the initial growth using the C_{24} cluster as a model. Reproduced with permission from Kang *et al.*, Carbon **181**, 225 (2021). Copyright 2021 Elsevier. (e)–(i) STM images of Si intercalated graphenes with different sizes; (j) energy levels simulation of a hexagonal graphene with a length from four carbon rings to eight carbon rings; (k) charge density simulation of the edge states near the Fermi level. Figures (e)–(k) are reproduced with permission from Chen *et al.*, Nano Res. **11**, 3722 (2018). Copyright 2018 ACS Publications. (l) The variation of energy of graphene wrinkles on Cu of different shapes; schematics of (m) strain distribution across a wrinkle and (n) the competition between wrinkled graphene and compressed flat graphene; structures of (o) epitaxial and (q) non-epitaxial graphene, total energy change of (p) epitaxial and (r) non-epitaxial graphene sliding in the horizontal (x) and vertical (y) directions on the surface of Cu(111). Figures (l)–(r) are reproduced with permission from Li *et al.*, Adv. Mater. **30**, 1706504 (2018). Copyright 2018 Wiley.



24 April 2024 17:19:13

FIG. 6. (a)–(f) Moiré pattern of graphene and graphene quantum dots on Ru(0001); (g) structures of graphene correspond to the local minima and the experimental results. Figures (a)–(g) are reproduced with permission from Zhu and Ding, *Nanoscale Horiz.* **4**, 625 (2019). Copyright 2019 Royal Society of Chemistry. (h) Synthesis mechanisms and (i) the first-principles simulations of graphene on Fe(100). Reproduced with permission from Hong *et al.*, *J. Phys. Chem. C* **123**, 26870 (2019). Copyright 2019 ACS Publications. (j) The optimized configuration of graphene on nickel. Reproduced with permission from Mafra *et al.*, *Phys. Rev. Mater.* **2**, 073404 (2018). Copyright 2018 American Physical Society.

for the fabrication of graphene. Thus, many calculations have been devoted to analyze the growth process of graphene. Based on spin-polarized ground-state density functional theory (SPGS-DFT) calculations, Vinogradov *et al.* studied the detailed atomic structure of

the graphene/Fe(110) interface with a simulation cell consisting of six flat layers of Fe atoms and graphene on top.⁷⁶ The calculated distances between graphene and Fe(110) surface around 2.7 Å are too short for breaking the C–Fe covalent bonds, indicating the

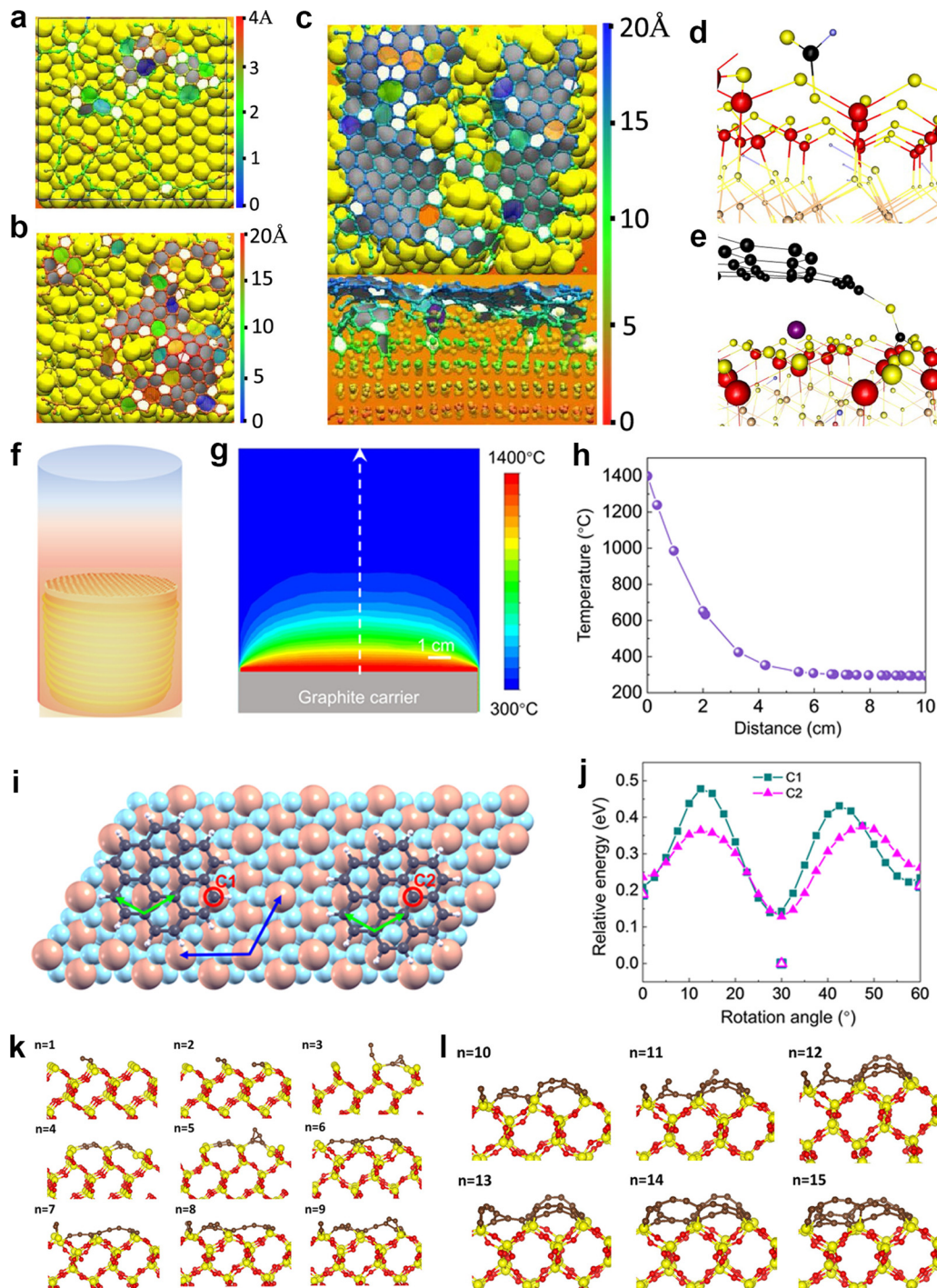


FIG. 7. The simulations of the graphene growth at (a) 2500 K and (b) 2600 K; (c) top and side views of the simulation of the graphene configuration at 2800 K. Figures (a)–(c) are reproduced with permission from Zhang *et al.*, Chem. Mater. **32**, 8306(2020). Copyright 2020 ACS Publications. (d) and (e) different structural selections pertinent to carbon transport on the surface of mica. Reproduced with permission from Lippert *et al.*, Carbon **52**, 40 (2013). Copyright 2013 Elsevier. (f)–(j) Mechanism of graphene alignment on the surface of Al₂O₃ (0001). Reproduced with permission from Chen *et al.*, Sci. Adv. **7**, eabk0115 (2021). Copyright 2021 The American Association for the Advancement of Science. (k) Optimized geometries of (C₂H₂)_n (n = 1–15) deposition on the surface of SiO₂ thermal oxide. Reproduced with permission from Longo *et al.*, ACS Appl. Mater. Interfaces **14**, 9492 (2022). Copyright 2022 ACS Publications.

strong interaction of graphene films with the substrate. Hong and co-workers created large supercells (1382 atoms) to estimate the interface between graphene and Fe surfaces through the *ab initio* density function theory including the VASP code and the SIESTA (Spanish Initiative for Electronic Simulations with Thousands of Atoms) method.¹²¹ The model structure of graphene grown on Fe revealed that the carbon states was polarized by the proximity effect near the Fermi level, as shown in Figs. 6(h) and 6(i).⁷⁷ A $10 \times 10 \times 1$ grid was adopted to sample the Brillouin zone under the Monkhorst–Pack scheme to perform relaxations with and without van der Waals interactions. As a result, the mechanism of thickness dependence was found relating to the amount of charge transfer from the Fe surface to graphene, and the Fermi level at the interface exhibited an oscillatory-like behavior with the layer thickness, saturating at approximately five layers, which fits well with the experimental data in Figs. 2(e) and 2(f) (2–5 layers).

Mafra and her co-workers combined the experimental and computational data of growing large-area single-layer graphene on the surfaces of Ni(111), Ni(110), and Ni(100), respectively.⁸⁰ DFT calculations implemented using the QUANTUM-ESPRESSO package¹²² and the PBE generalized gradient approximation as exchange-correlation functional were performed. As shown in Fig. 6(j), the computational simulations revealed that graphene growth on the surface of Ni(111) showed a planar structure, and the graphene growth on Ni(110) suggested that the formation of carbide is slightly disfavored (only 0.09 eV), both of which fit well with the results shown in Figs. 2(g) and 2(h). For the purpose of combining the advantages of Ni and Cu, CuNi alloys were also applied as the substrates to develop large-area single-crystalline graphene with fast growth rate and low nucleation density for recent years. Wu *et al.* grew 1.5-in.-large graphene monolayer in 2.5 h using an optimized CuNi alloy as the substrate.¹²³ DFT calculations implemented in the VASP were performed. The formation of a Ni atomic chain into the Cu bulk was found that it could significantly lower the formation energy of a C interstitial atom from 3 to 1 eV, ensuring an easier migration along a Ni chain in the alloy, which could explain the phenomenon in Ref. 82.

B. DFT method to calculate graphene/non-metal interaction

1. Calculations involving non-metallic substrates with weak interaction

Because of the complex kinetic and thermodynamic processes for the epitaxial growth of graphene on SiC substrates, an urgent need for accurate and suitable calculations has arisen in recent years. Yu *et al.* performed an *ab initio* molecular dynamics (AIMD) simulation using the VASP method to estimate the graphene growth on the surface of SiC (1 $\bar{1}$ 00) at 1000 °C, aiming to understand the transformation from three-layer SiC to monolayer graphene.¹²⁴ It was demonstrated that less stable carbon clusters and a network formed as transition structures in sublimation procedure of the first and second layers, while a large-area single-layer graphene could be observed during the sublimation of the third SiC layer. The current ReaxFF Si/H/graphene force field development with the standalone ReaxFF code and all MD/fbMC simulations using ReaxFF module of parallel ADF package¹²⁵ were performed by Zhang and van Duin

for the purpose of studying molecular dynamics (MD) at the atomistic level of graphene growth on the SiC substrate.¹²⁶ Thermal decomposition was demonstrated as an effective factor for graphene growth [Figs. 7(a)–7(c)], and detailed dynamics information proposed that multi-layer graphene is usually synthesized on the C-terminated surface while single-layer graphene is easily generated on Si-terminated SiC surface shown in Fig. 7(c), which fits well with the common experimental practice.

The *ab initio* DFT using Quantum Espresso was performed by Lippert *et al.* for the calculations of energy barriers, atomic structures, total energies, and molecular dynamics, to investigate the van der Waals growth of graphene on the mica surface by the molecular beam epitaxy (MBE) method.⁸⁵ The larger physisorption energy indicated that the van der Waals–Debye force promoted smaller flakes adhesion. The molecular dynamics at 700 °C showed that even large molecules (e.g., C₂₄) could slide on the flat mica surface with no barrier. Due to the unique performances of graphene growth on the mica surface, they carried out further work to detect the proper processing window for the fabrication of high qualified graphene.⁹⁰ As shown in Figs. 7(d) and 7(e), the reaction occurred between the atomic carbon and mica surface revealed that oxygen did not escape from the surface of mica and remain bonded in formyl moieties. The presence of oxygen on the edge of graphene molecules was helpful for the collection of C atoms from defects, which was an important factor of growing graphene with high quality on the mica surface, as shown in Figs. 3(e) and 3(f).

It is well known that guiding the graphene domains into good alignment could minimize its configuration energy effectively. Thus, first-principles calculations based on DFT were carried out to reveal the preferable orientation of the graphene growth on sapphire (Al₂O₃) in the process of electromagnetic induction heating CVD,⁹³ and demonstrated that the most stable orientation of graphene on a sapphire (0001) substrate could be observed when the rotational angle is 30°, as shown in Figs. 7(f)–7(j). Park and co-workers carried out the calculations (64 Al atoms and 96 O atoms) using the VASP and PAW method with an energy cut-off of 500 eV,⁹⁴ indicating the associated barrier of the minimum energy path in this way was negligible ($E_d \approx 0$ eV), which was comparable to the barrier on Cu (~ 0.07 eV),¹²⁷ ensuring the successful synthesis of high-quality graphene.

Longo and Ventzek applied DFT coupled with AIMD methods to study the initial stages of graphene growth on the SiO₂ surface using C₂H₂ as the PE-CVD precursor.¹²⁸ As shown in Fig. 7(k), the calculations demonstrated that the formation of Si–C₂ bonds at the beginning sets as the nucleation center for the growth of the carbon layer. And, further formation of Si–C–C–Si bridge bonds turned out to be a thermodynamically exothermic process, which promoted generation of pinning center and the second-row carbon dimers starting from (C₂H₂)₅ and (C₂H₂)₉, respectively. Finally, this process could produce a stable and planar graphene. Xie *et al.* found an effective way of growing wafer-scale graphene on SiO₂ through a local-fluorine-supply method.¹²⁹ Further DFT based first-principles calculations demonstrated that the released fluorine from the fluoride substrate at high temperatures can rapidly react with CH₄ to form CH₃F with higher activity, which lowered the barrier of carbon attachment, providing sufficient carbon feedstock for graphene CVD growth.

24 April 2024 17:19:13

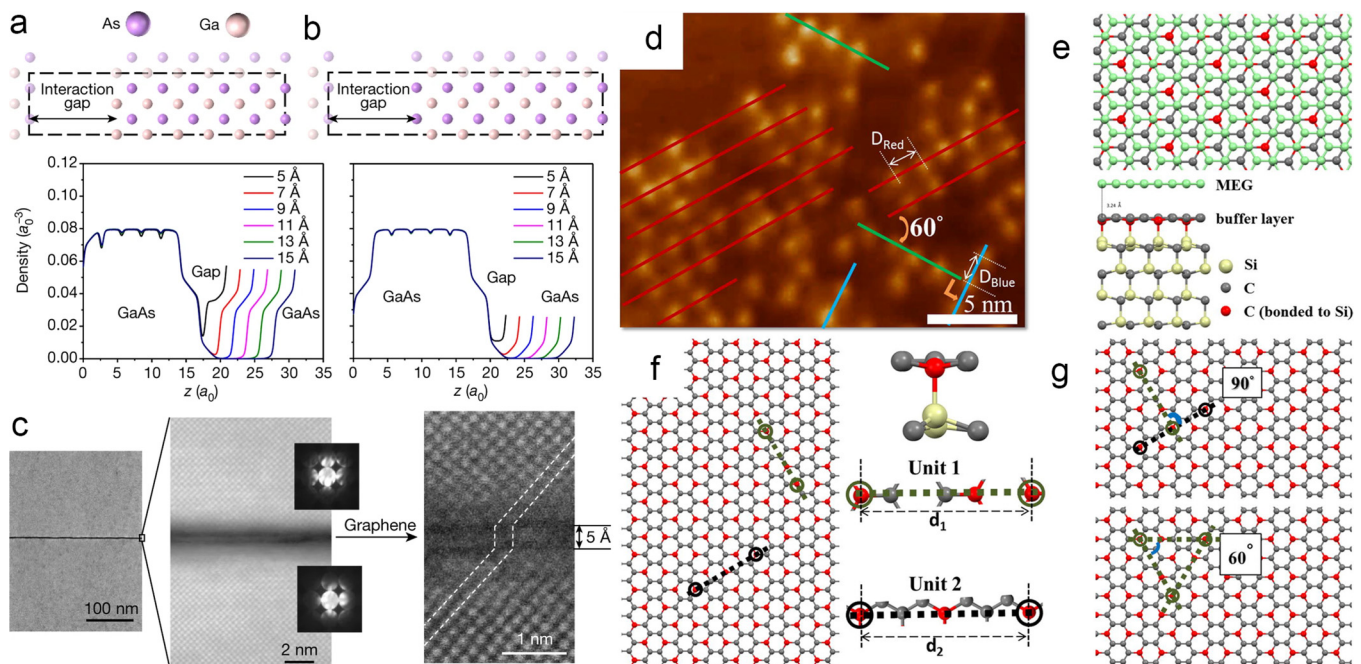


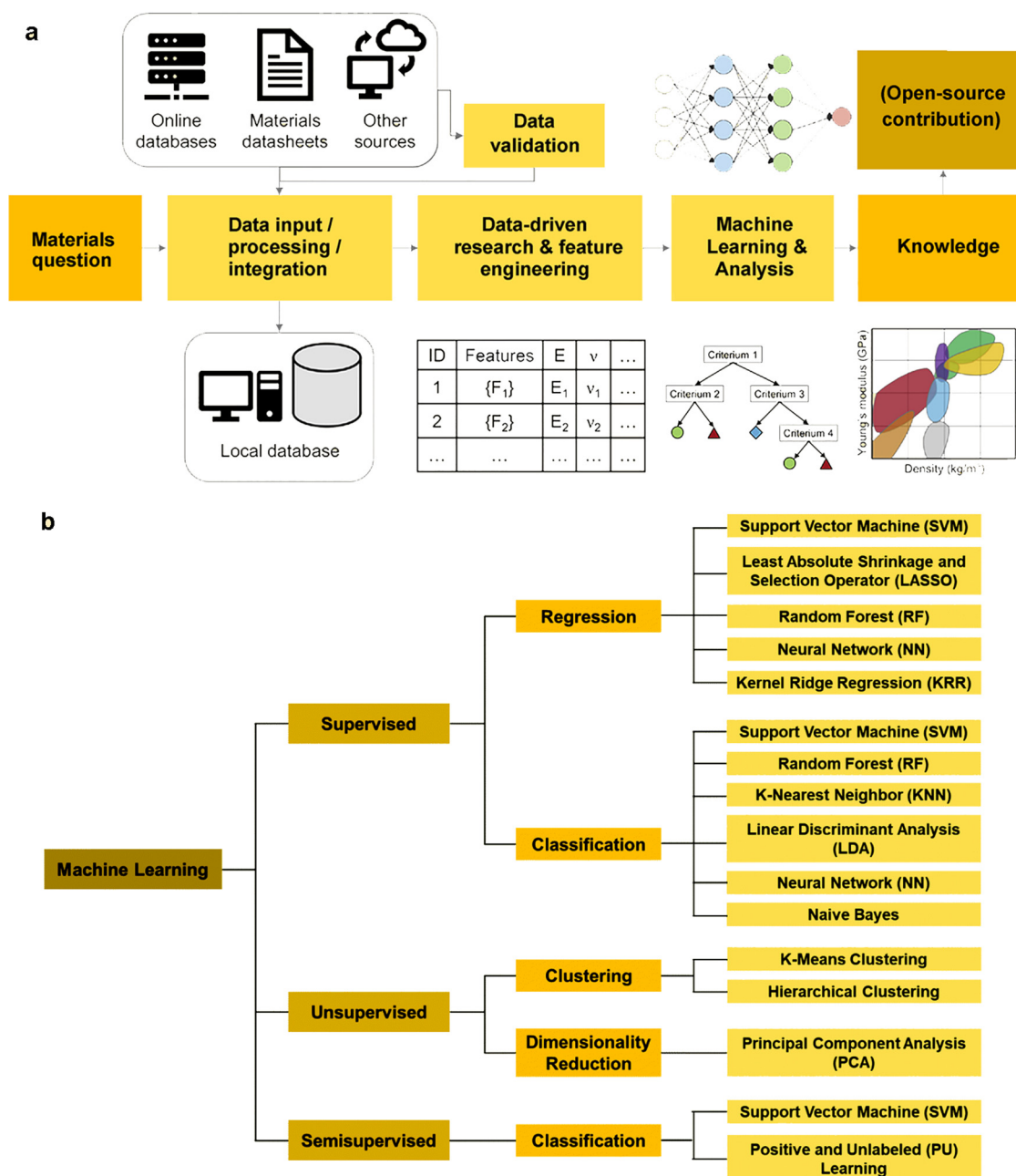
FIG. 8. DFT calculated results for averaged electron density along GaAs slabs for (a) As–Ga and (b) As–As interactions, (c) STEM images of the GaAs(001) lattice alignment through graphene. Reproduced with permission from Kim *et al.*, *Nature* **544**, 340 (2017). Copyright 2017 Springer. (d) The practical linear Bi arrangements, (e) top view and side view of schematic MEG (graphene)/4H-SiC (0001), (f) and (g) DFT calculations of Bi adatoms on graphene. Reproduced with permission from Chen *et al.*, *Carbon* **93**, 180 (2015). Copyright 2015 Elsevier.

2. Calculations involving epitaxy of materials through graphene coated substrate

Chen *et al.* provided a fundamental theory of understanding epitaxy combining experimental and computational data, which revealed that the features of heterointerface mainly relied on both the feature of growth material and the underlying substrate.¹³⁰ DFT calculations using VASP with PBE applied for the exchange-correlation function were performed, and concluded that the van der Waals heterointerface (polycrystalline) was the main structure when grown on amorphous substrates, while the heterointerface would inherit the substrate's lattice and behave like a covalent one for single-crystalline substrates, which explained the single-crystalline epitaxy in Fig. 4(a). Kim and co-workers also realized homoepitaxial growth of GaAs(001) on GaAs(001) substrates accommodated by a single-layer graphene, which was also applicable to InP and GaP.⁹⁸ They chose As-termination of GaAs(001) slabs as the computational model, and the interaction of Ga- and As-terminated layers of GaAs on the As-terminated substrate was calculated by DFT computation using the plane-wave pseudopotential code as implemented in Quantum Espresso. As shown in Figs. 8(a) and 8(b), when the gap was beyond about 9 Å, significant charge density between the separated GaAs slabs disappeared, suggesting possibility of occurrence for remote epitaxy within a 9 Å gap between epilayer and substrate. Actually, the measured distance between the substrate and the GaAs epilayer was 5 Å [Fig. 8(c)], which fits well with the results of DFT calculations.

In addition, the epitaxy of single-element thin film through the graphene coated substrate also attracted much attention. A bond-order potential was proposed by Forster and Rabilloud for the C–Ru system, for the purpose of modeling Ru nanoparticles on such substrates or graphene.¹³¹ The local optimizations and molecular dynamics simulations were applied to address the thermal and energetic stabilities of Ru nanoparticles on the surface of epitaxial graphene. And it was found that Ru nanoparticles could be stabilized by the corrugation of epitaxial graphene against global diffusion and internal rearrangement. With the actual observation of STM, DFT calculations under the local density approximation potential (LDA) implemented in the VASP codes were performed by Chen *et al.* to study the growth of Bi on monolayer graphene, as shown in Figs. 8(d)–8(g).¹³² They demonstrated that the underlying buffer layer of SiC could determine the effect of corrugated substrate, causing different linear arrangements of Bi adatoms, even across the block of graphene. Two different bonding length of the buffer layer ($d_1/d_2 \approx 0.866$) calculated through DFT fitted well with statistical length ratio ($D_{\text{Red}}/D_{\text{Blue}} \approx 0.878 \pm 0.008$) extracted from experimental data [Figs. 8(d) and 8(f)]. Finally, the buffer layer was assumed to be an important factor of forming the linear Bi structure, and both the effect of the corrugated surface of SiC substrate and the mediation of graphene Dirac-like electrons resulted in the oscillatory interaction.

As discussed above, enormous progresses of DFT method calculating the interaction on the epitaxy of graphene were achieved

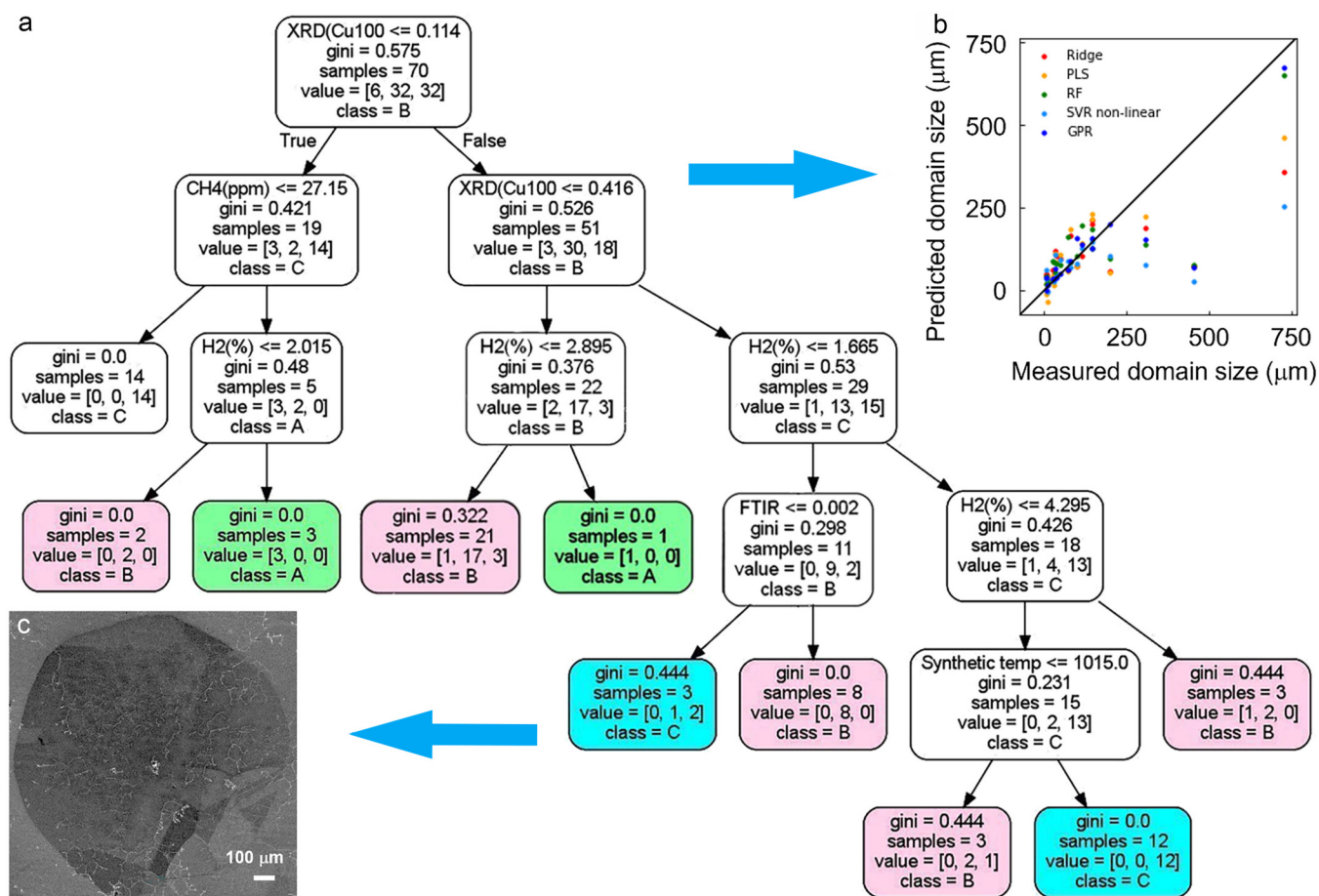


24 April 2024 17:19:13

FIG. 9. (a) Schematic of employing a general machine learning process in materials science. Reproduced with permission from Wang *et al.*, Chem. Mater. **32**, 4954 (2020). Copyright 2020 ACS Publications. (b) ML algorithms applied in 2D materials. Reproduced with permission from Ryu *et al.*, Chem. Soc. Rev. **51**, 1899 (2022). Copyright 2022 Royal Society of Chemistry.

in the recent decades. However, significant obstacles remain including the relative low accuracy and small computation capacity (number of atoms). In detail, the absence of accurate description of vdW interaction results in the low accuracy for describing the

complicate interaction. For example, Li *et al.* found that five commonly used DFT-based vdW models could not explain the experimental results of vdW interactions at graphite, MoS₂, and BN interfaces.¹³³ In addition, the limitation of the model size existed in



24 April 2024 17:19:13

FIG. 10. (a) Visualization of decision tree regression; (b) measured and predicted sizes of d_{domain} for five different models of ML; (c) SEM images of graphene grown using the predicted experimental conditions through ML. Reproduced with permission from Yoshihara *et al.*, J. Chem. Eng. e2911 (2023). Copyright 2021 Wiley.

DFT methods caused the unclear growth mechanisms, because the small computation capacity hinders the exploration of graphene growth with large-area. Thus not only more accurate calculations involving improvement of algorithms and mechanisms of interactions, but also more effective models as well as much larger calculated quantity are urgently required. Actually, due to the mathematically well-defined procedure and increasingly larger number of easy-to-use packages for modeling atomistic system, machine learning (ML) methods have shown remarkable potential of solving the problem, which will now be discussed in detail.

C. Machine learning method to train model and potential

Recent progresses in atomically thin 2D materials, such as graphene, hexagonal boron nitride nanosheet (h-BNNS), MoS₂, etc., have led to a great deal of technologies with promising potential in the optoelectronics, photonics, and energy fields.^{134,135} However, serious issues related to materials quality hinder their practical

applications, and the different structure due to the variety of growth procedure will influence their properties significantly.¹³⁶ Mounet *et al.* proposed an existence possibility of nearly 2000 kinds of 2D materials through DFT calculations in 2018,¹³⁷ but there will invariably be high cost and substantial human resources required if each of the materials are explored through conventional experimental approaches. Unfortunately, conventional experimental and computational approaches (first-principles calculations, such as DFT) can scarcely keep up with the rapidly growing demands in the study of 2D materials. In addition, both experimental methods and computational simulations using first-principles calculations, such as high throughput DFT, require considerable time and cost, which slows progress in 2D materials study. Hence, an advanced strategy with precise computational prediction is urgently required to optimize the experimental design for practical applications. Machine learning (ML)-based prediction can be a viable and optimal approach to accurately point out the possible synthesizability of 2D materials, and the fast development of low-cost computation, data sources, and new machine learning algorithms theories

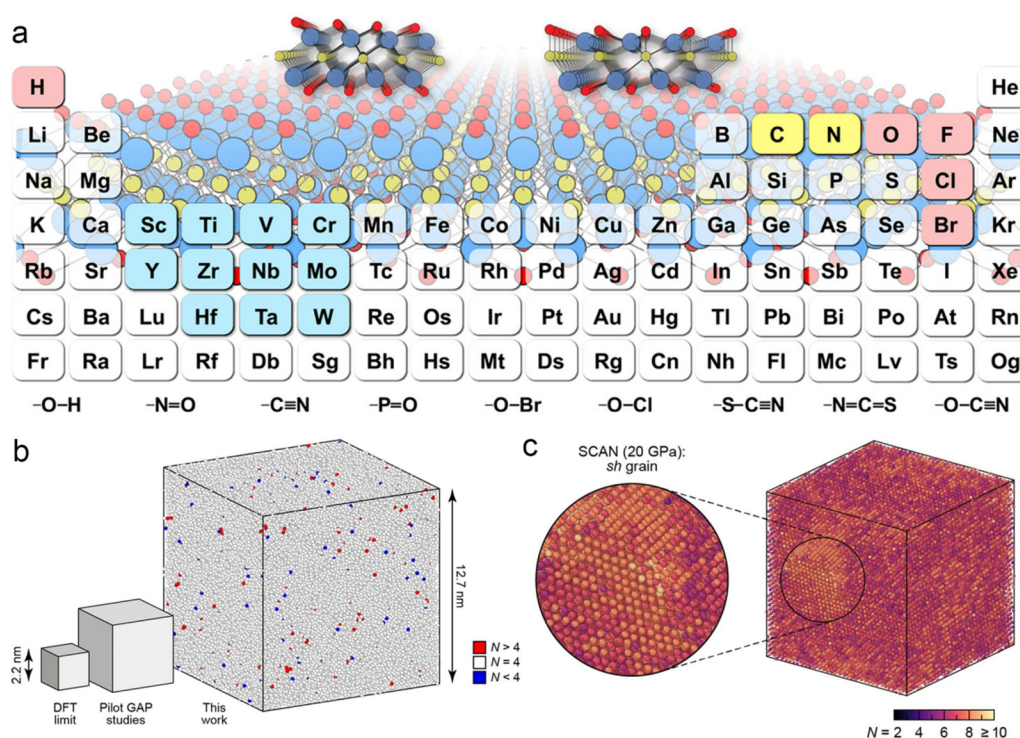


FIG. 11. (a) A group of 23 870 MXenes generated through early transition metals and surface functional groups. Reproduced with permission from Rajan *et al.*, Chem. Mater. **30**, 4031 (2018). Copyright 2018 ACS Publications. (b) ML-driven modeling (a Si structure with 100 000 atoms) beyond the nanometric length scale, (c) oblique view of the simulation cell from the ML simulation. Reproduced with permission from Deringer *et al.*, Nature **589**, 59 (2021). Copyright 2021 Springer.

have stimulated the application of ML.^{138,139} Using the chemical and physical performances of simulated and already-known 2D materials, ML models could not only propose effective interpretations for complicated interconnections and correlations among the properties, but also make predictions of unknown features of new-unknown 2D materials. Moreover, ML algorithms with more training can make quicker and more accurate predictions, enabling ML a promising strategy for understanding, design, and synthesis of 2D materials.

The most important part of ML-assisted design is the effective training of ML models. A simplified schematic diagram of applying ML into materials science was shown in Fig. 9(a).¹⁴⁰ Actually, the target (material properties or classes), the descriptor(s) of features, and the choice of algorithms and hyper-parameters are the key factors of basic ML model training, which can be expressed as:^{46,141}

$$\text{Data}(\text{Target} + \text{Descriptors}) + \text{Algorithms} + \text{Hyper-parameters} = \text{ML Model}.$$

As shown in Fig. 9(b), ML techniques can be divided into three categories according to the handled data: supervised, unsupervised, and semisupervised learning.¹⁴² While supervised learning is the procedure of finding a mapping function, unsupervised

learning tries to resolve new patterns and distribution from unlabeled data, and semisupervised learning turns out to be a practical model for managing practical classification and clustering problems associated with predicting outcomes based on a dearth of correct information. Support vector machine (SVM), least absolute shrinkage and selection operator (LASSO), random forest (RF), neural network (NN), K-Means, and principal component analysis (PCA) are the representative ML algorithms, and a common strategy is to train a couple of ML models and estimate their features.

According to the discussion in Sec. I A, using the Cu substrate turns out to be a promising way to grow large-area graphene with high quality. Thus, Yoshihara and co-workers designed a ML model to explore optimized experimental CVD conditions for the graphene growth on the Cu foils,¹⁴³ six types of ML models including Gaussian process regression (GPR), support vector regression (SVR), random forest (RF), partial least squares (PLS), decision tree regression (DTR), and ridge regression (RR) were employed to simulate the graphene growth conditions. The dataset comprised of 88 experiments with the XRD profile and FTIR spectrum results were applied to train the ML models, respectively. For example, the visualization of the DTR model was shown in Fig. 10(a), and the data points was sorted accurately by the simple decision rules based on inequalities. Owing to its complexity, the GPR model showed the highest accuracy among models [Fig. 10(b)]. The proposed

experimental conditions by conducting the actual graphene growth by CVD was proved to realize the graphene domains with lateral sizes as high as 1.3 mm in practical experiments, as presented in Fig. 10(c).

Due to the coupled and complex relationship of the composition of solvents, concentration of precursors, the reaction time and temperature, Du *et al.*¹⁴⁴ found that the large-scale synthesis process of uniform ultrathin 2D films was difficult to discover the relationship between those parameters and the material structure. It is found that the poor understanding of growth mechanisms for materials synthesis hinders the structure prediction. For instance, MXene is a popular 2D material, and its change of compositions results in different properties for plentiful applications. By applying different ML models including GPR, KRR, SVR, and BAR (bootstrap aggregating regression) algorithms, Rajan *et al.* calculated the bandgaps of MXenes to study the electronic properties of MXenes. More than 23 800 kinds of MXenes were developed according to their compositions [Fig. 11(a)].¹³⁹ 76 MXenes simulated with DFT (PBE method) were selected to build the prediction models, and the GPR model showed the most accurate bandgap prediction. However, due to the small dataset of only 76 samples, the results may be not convincing enough. In addition, it worth noting that many materials which was predicted to exist might not be synthesizable through modern technologies. Although the existence of over 23 800 MXenes had been predicted by theoretical calculations (e.g., MD, DFT), only about 20 kinds of MXenes have been successfully synthesized.¹⁴⁵ To solve those problems, ML has been thought as a promising way to predict synthesizable candidates and understand the complex relationships between them.

Besides the ML model for prediction, the ML potentials were trained for the purpose of highly accurate molecular dynamics simulations, an interatomic potential for graphene was constructed by Rowe *et al.* to generate a more accurate ML interatomic potential,¹⁴⁶ comparing the capabilities of modern ML algorithms with those of empirical many-body potentials (the prediction of atomic forces using DFT and thermal expansion of graphene using AIMD simulations). As a result, a computational cost in orders of magnitude lower than that of comparable calculations was also achieved. Aiming to pursue an in-depth understanding of the structural transitions of disordered silicon, atomistic ML methods were constructed by Deringer *et al.* on accurate quantum mechanical computations in the case of the accessible system sizes (tens of nanometer length scale, about 100 000 atoms) via calculation, which was much larger than the DFT methods, as shown in Figs. 11(b) and 11(c).¹⁴⁷

In brief, a better understanding of the complex relationships, with the help of experiments, simulations, and ML, will promote the development of high-efficiency and large-area 2D material synthesis technology, enabling mass production. The advanced ML methods could be applied to identify trends of many material structures according to the already-known data. The ML potentials could break through the size limitation of conventional DFT calculations to reveal the unclear growth mechanisms. However, the ML method also faces obstacles including small quantities of data, lack of efficient training, and accuracy of results *etc.* Thus, great efforts are urgently required to break the bottleneck of the current ML methods in understanding epitaxy of graphene.

IV. PERSPECTIVE

The fabrication methodologies of graphenes, especially the epitaxial growth strategies, were discussed using both the experimental and computational results in this perspective. Practical examples were listed and summarized through different substrates (metal and non-metal) in terms of the interaction strength, involving van der Waals interaction and covalent bonding. How to design a model according to the actual generating conditions of graphene (even other 2D materials) has attracted much attention, and many of computing results fit well with practical circumstance. The DFT calculations have provided effective guidance for mechanism interpretation of growing procedure as well as the complex interaction between graphene and substrates. However, the main obstacles including the relative low accuracy and small computation capacity have not been addressed yet, which call for more accurate algorithms, more effective methods, and much larger calculated quantity. In this perspective, we proposed that machine learning (ML) methods have the remarkable potential of solving the problems discussed above due to the mathematically well-defined procedure and increasingly larger number of easy-to-use packages for modeling atomistic systems. Actually, ML has been applied in the fabrication of 2D materials for many years, and a few reports about excellent results based on ML algorithms for the epitaxial growth of graphene also show the great potential in this field. Thus, advanced computing methods and ML strategies should be put forward to accelerate the development of graphene as well as other 2D materials.

ACKNOWLEDGMENTS

We acknowledge support from the National Natural Science Foundation of China (NNSFC) (Nos. 92266105 and 51705017).

AUTHOR DECLARATIONS

Conflicts of Interest

The authors have no conflicts to disclose.

Author Contributions

Ming-Sheng Zheng: Funding acquisition (equal); Project administration (lead); Writing – original draft (lead). **Shaojie Zhou:** Visualization (lead). **Xinmo Wang:** Investigation (equal). **Lei Gao:** Funding acquisition (equal); Investigation (equal); Supervision (lead); Writing – review & editing (lead).

DATA AVAILABILITY

The data that support the findings of this study are available from the corresponding author upon reasonable request.

REFERENCES

- ¹R. E. Peierls, *Helv. Phys. Acta* **7**, 81 (1934).
- ²L. D. Landau, *Phys. Z. Sowjetunion* **11**, 26 (1937).
- ³K. S. Novoselov, A. K. Geim, S. V. Morozov, D. Jiang, Y. Zhang, S. V. Dubonos, I. V. Grigorieva, and A. A. Firsov, *Science* **306**, 666–669 (2004).
- ⁴H. Tetlow, J. P. De Boer, I. J. Ford, D. D. Vvedensky, J. Coraux, and L. Kantorovich, *Phys. Rep.* **542**, 195–295 (2014).

- ⁵N. Kumar, R. Salehiyan, V. Chauke, O. J. Botlhoko, K. Setshedi, M. Scriba, M. Masukume, and S. S. Ray, *FlatChem* **27**, 100224 (2021).
- ⁶M. H. Gass, U. Bangert, A. L. Bleloch, P. Wang, R. R. Nair, and A. K. Geim, *Nat. Nanotechnol.* **3**, 676–681 (2008).
- ⁷X. Du, I. Skachko, A. Barker, and E. Y. Andrei, *Nat. Nanotechnol.* **3**, 491–495 (2008).
- ⁸J.-H. Chen, C. Jang, S. Xiao, M. Ishigami, and M. S. Fuhrer, *Nat. Nanotechnol.* **3**, 206–209 (2008).
- ⁹A. Akturk and N. Goldsman, *J. Appl. Phys.* **103**, 053702 (2008).
- ¹⁰A. A. Balandin, S. Ghosh, W. Bao, I. Calizo, D. Teweldebrhan, F. Miao, and C. N. Lau, *Nano Lett.* **8**, 902–907 (2008).
- ¹¹C. Lee, X. Wei, J. W. Kysar, and J. Hone, *Science* **321**, 385–388 (2008).
- ¹²A. F. Carvalho, B. Kulyk, A. J. S. Fernandes, E. Fortunato, and F. M. Costa, *Adv. Mater.* **34**, 2101326 (2022).
- ¹³A. G. Olabi, M. A. Abdelkareem, T. Wilberforce, and E. T. Sayed, *Renew. Sust. Energy Rev.* **135**, 110026 (2021).
- ¹⁴A. Razaq, F. Bibi, X. Zheng, R. Papadakis, S. H. M. Jafri, and H. Li, *Materials* **15**, 1012 (2022).
- ¹⁵R. S. Edwards and K. S. Coleman, *Nanoscale* **5**, 38–51 (2013).
- ¹⁶M. Lotya, P. J. King, U. Khan, S. De, and J. N. Coleman, *ACS Nano* **4**, 3155–3162 (2010).
- ¹⁷R. J. Smith, M. Lotya, and J. N. Coleman, *New J. Phys.* **12**, 125008 (2010).
- ¹⁸W. Fu, J. Kiggans, S. H. Overbury, V. Schwartz, and C. Liang, *Chem. Commun.* **47**, 5265 (2011).
- ¹⁹A. Safavi, M. Tohidi, F. A. Mahyari, and H. Shahbaazi, *J. Mater. Chem.* **22**, 3825 (2012).
- ²⁰M. Yi and Z. Shen, *J. Mater. Chem. A* **3**, 11700–11715 (2015).
- ²¹M. An, J. Wu, P. Wang, and Y. Fang, *Appl. Phys. Lett.* **114**, 022102 (2019).
- ²²B. C. Brodie, *Philos. Trans. R. Soc. London* **149**, 249–259 (1859).
- ²³L. Staudenmaier, *Ber. Dtsch. Chem. Ges.* **31**, 1481–1487 (1898).
- ²⁴W. S. Hummers and R. E. Offeman, *J. Am. Chem. Soc.* **80**, 1339 (1958).
- ²⁵D. A. C. Brownson and C. E. Banks, *Analyst* **135**, 2768 (2010).
- ²⁶P. W. Sutter, J.-I. Flege, and E. A. Sutter, *Nat. Mater.* **7**, 406–411 (2008).
- ²⁷W. Norimatsu and M. Kusunoki, *Phys. Chem. Chem. Phys.* **16**, 3501 (2014).
- ²⁸L. Gao, J. R. Guest, and N. P. Guisinger, *Nano Lett.* **10**, 3512–3516 (2010).
- ²⁹K. S. Novoselov, D. Jiang, F. Schedin, T. J. Booth, V. V. Khotkevich, S. V. Morozov, and A. K. Geim, *Proc. Natl. Acad. Sci. U.S.A.* **102**, 10451–10453 (2005).
- ³⁰T. Seyller, A. Bostwick, K. V. Emtsev, K. Horn, L. Ley, J. L. McChesney, T. Ohta, J. D. Riley, E. Rotenberg, and F. Speck, *Phys. Status Solidi (B)* **245**, 1436–1446 (2008).
- ³¹K. Yang, W. D. Xiao, Y. H. Jiang, H. G. Zhang, L. W. Liu, J. H. Mao, H. T. Zhou, S. X. Du, and H.-J. Gao, *J. Phys. Chem. C* **116**, 14052–14056 (2012).
- ³²X. Wang, H. Guo, J. Lu, H. Lu, X. Lin, C. Shen, L. Bao, S. Du, and H. J. Gao, *Chin. Phys. B* **30**, 048102 (2021).
- ³³S. Gottardi, K. Müller, L. Bignardi, J. C. Moreno-López, T. A. Pham, O. Ivashenko, M. Yablonskikh, A. Barinov, J. Björk, P. Rudolf, and M. Stöhr, *Nano Lett.* **15**, 917–922 (2015).
- ³⁴Y. Que, W. Xiao, X. Fei, H. Chen, L. Huang, S. X. Du, and H.-J. Gao, *Appl. Phys. Lett.* **104**, 093110 (2014).
- ³⁵X. He, Q. Bai, and R. Shen, *Carbon* **130**, 672–679 (2018).
- ³⁶Y. Chen, J. Wang, P. Schützendübe, Z. Wang, and E. J. Mittemeijer, *Carbon* **159**, 37–44 (2020).
- ³⁷I. Shtepliuk, F. Giannazzo, and R. Yakimova, *Appl. Sci.* **11**, 5784 (2021).
- ³⁸A. N. Rudenko, F. J. Keil, M. I. Katsnelson, and A. I. Lichtenstein, *Phys. Rev. B* **83**, 045409 (2011).
- ³⁹J. Shan, J. Sun, and Z. Liu, *ChemNanoMat* **7**, 515–525 (2021).
- ⁴⁰S. Wei, L.-P. Ma, M.-L. Chen, Z. Liu, W. Ma, D.-M. Sun, H.-M. Chen, and W. Ren, *Carbon* **148**, 241–248 (2019).
- ⁴¹S. Naghdi and V. Mišković-Stanković, “A review of the corrosion behaviour of graphene coatings on metal surfaces obtained by chemical vapour deposition,” *J. Electrochem. Soc.* **169**, 021505 (2022).
- ⁴²S. Haghghatpanah, A. Börjesson, H. Amara, C. Bichara, and K. Bolton, *Phys. Rev. B* **85**, 205448 (2012).
- ⁴³L. L. Patera, F. Bianchini, C. Africh, C. Dri, G. Soldano, M. M. Mariscal, M. Peressi, and G. Comelli, *Science* **359**, 1243–1246 (2018).
- ⁴⁴Y. Li, M. Li, T. Wang, F. Bai, and Y.-X. Yu, *Phys. Chem. Chem. Phys.* **16**, 5213 (2014).
- ⁴⁵K. T. Butler, D. W. Davies, H. Cartwright, O. Isayev, and A. Walsh, *Nature* **559**, 547–555 (2018).
- ⁴⁶G. R. Schleder, A. C. M. Padilha, C. M. Acosta, M. Costa, and A. Fazzio, *J. Phys. Mater.* **2**, 032001 (2019).
- ⁴⁷J. Schmidt, M. R. G. Marque, S. Botti, and M. A. L. Marques, *npj Comput. Mater.* **5**, 83 (2019).
- ⁴⁸P. Wu, W. Zhang, Z. Li, and J. Yang, *Small* **10**, 2136–2150 (2014).
- ⁴⁹C. Si, Z. Sun, and F. Liu, *Nanoscale* **8**, 3207–3217 (2016).
- ⁵⁰D. Y. Usachov, V. Y. Davydov, V. S. Levitskii, V. O. Shevelev, D. Marchenko, B. V. Senkovskiy, O. Y. Vilkov, A. G. Rybkin, L. V. Yashina, E. V. Chulkov, I. Y. Sklyadneva, R. Heid, K. P. Bohnen, C. Laubschat, and D. V. Vyalikh, *ACS Nano* **11**, 6336–6345 (2017).
- ⁵¹L. Meng, J. Lu, Y. Bai, L. Liu, J. Tang, and X. Zhang, *Phys. Chem. Chem. Phys.* **23**, 2222–2228 (2021).
- ⁵²H. C. Lee, W.-W. Liu, S.-P. Chai, A. R. Mohamed, A. Aziz, C.-S. Khe, N. M. S. Hidayat, and U. Hashim, *RSC Adv.* **7**, 15644–15693 (2017).
- ⁵³V. Yong and H. T. Hahn, *CrystEngComm* **13**, 6933 (2011).
- ⁵⁴J. Sun, Y. Nam, N. Lindvall, M. T. Cole, K. B. K. Teo, Y. Woo Park, and A. Yurgens, *Appl. Phys. Lett.* **104**, 152107 (2014).
- ⁵⁵J. Ping and M. S. Fuhrer, *J. Appl. Phys.* **116**, 044303 (2014).
- ⁵⁶A. B. Preobrajenski, M. L. Ng, A. S. Vinogradov, and N. Mårtensson, *Phys. Rev. B* **78**, 073401 (2008).
- ⁵⁷L. Meng, R. Wu, L. Zhang, L. Li, S. Du, Y. Wang, and H.-J. Gao, *J. Phys.: Condens. Matter* **24**, 314214 (2012).
- ⁵⁸P. Merino, M. Svec, A. L. Pinardi, G. Otero, and J. A. Martin-Gago, *ACS Nano* **5**, 5627–5634 (2011).
- ⁵⁹P. Sutter, J. T. Sadowski, and E. Sutter, *Phys. Rev. B* **80**, 245411 (2009).
- ⁶⁰R. Balog, B. Jørgensen, L. Nilsson, M. Andersen, E. Rienks, M. Bianchi, M. Fanetti, E. Lægsgaard, A. Baraldi, S. Lizzit, Z. Sljivancanin, F. Besenbacher, B. Hammer, T. G. Pedersen, P. Hofmann, and L. Hornekaer, *Nat. Mater.* **9**, 315–319 (2010).
- ⁶¹C. Vo-Van, A. Kimouche, A. Reserbat-Plantey, O. Fruchart, P. Bayle-Guillemaud, N. Bendiab, and J. Coraux, *Appl. Phys. Lett.* **98**, 181903 (2011).
- ⁶²J. Coraux, M. Engler, C. Busse, D. Wall, N. Buckanie, F. J. M. Heringdorf, R. V. Gastel, B. Poelsema, and T. Michely, *New J. Phys.* **11**, 023006 (2009).
- ⁶³G. A. López and E. J. Mittemeijer, *Scr. Mater.* **51**, 1–5 (2004).
- ⁶⁴M. Wang, D. Luo, B. Wang, and R. S. Ruoff, *Trends Chem.* **3**, 15–33 (2021).
- ⁶⁵X. Li, W. Cai, L. Colombo, and R. S. Ruoff, *Nano Lett.* **9**, 4268–4272 (2009).
- ⁶⁶S. Chen, H. Ji, H. Chou, Q. Li, H. Li, J. W. Suk, R. Piner, L. Liao, W. Cai, and R. S. Ruoff, *Adv. Mater.* **25**, 2062–2065 (2013).
- ⁶⁷J. Wang, W. Bo, Y. Ding, X. Wang, and X. Mu, *Mater. Today Phys.* **14**, 100238 (2020).
- ⁶⁸L. Zhang, J. Dong, Z. Guan, X. Zhang, and F. Ding, *Nanoscale* **12**, 12831–12839 (2020).
- ⁶⁹Y. Pan, M. Gao, L. Huang, F. Liu, and H.-J. Gao, *Appl. Phys. Lett.* **95**, 093106 (2009).
- ⁷⁰K. Donner and P. Jakob, *J. Chem. Phys.* **131**, 164701 (2009).
- ⁷¹J. Halle, N. Néel, and J. Kröger, *J. Phys. Chem. Lett.* **12**, 6889–6894 (2021).
- ⁷²B. Wang, M.-L. Bocquet, S. Marchini, S. Günther, and J. Winterlin, *Phys. Chem. Chem. Phys.* **10**, 3530 (2008).
- ⁷³W. Moritz, B. Wang, M.-L. Bocquet, T. Brugger, T. Greber, J. Winterlin, and S. Günther, *Phys. Rev. Lett.* **104**, 136102 (2010).
- ⁷⁴K. F. McCarty, P. J. Feibelman, E. Loginova, and N. C. Bartelt, *Carbon* **47**, 1806–1813 (2009).
- ⁷⁵Y. Xue, B. Wu, Y. Guo, L. Huang, L. Jiang, J. Chen, D. Geng, Y. Liu, W. Hu, and G. Yu, *Nano Res.* **4**, 1208–1214 (2011).

- ⁷⁶N. A. Vinogradov, A. A. Zakharov, V. Kocovski, J. Ruzs, K. A. Simonov, O. Eriksson, A. Mikkelsen, E. Lundgren, A. S. Vinogradov, N. Mårtensson, and A. B. Preobrajenski, *Phys. Rev. Lett.* **109**, 026101 (2012).
- ⁷⁷J. Hong, Y. Kim, J. Liang, H. Chen, C. Y. Park, H. Yang, E. J. G. Santos, J. Bokor, C. C. Hwang, and L. You, *J. Phys. Chem. C* **123**, 26870–26876 (2019).
- ⁷⁸F. Mittendorfer, A. Garhofer, J. Redinger, J. Klime, J. Harl, and G. Kresse, *Phys. Rev. B* **84**, 201401 (2011).
- ⁷⁹Y. Gamou, A. Nagashima, M. Wakabayashi, M. Terai, and C. Oshima, *Surf. Sci.* **374**, 61–64 (1997).
- ⁸⁰D. L. Mafra, J. A. Olmos-Asar, F. R. Negreiros, A. Reina, K. K. Kim, M. S. Dresselhaus, J. Kong, G. J. Mankey, and P. T. Araujo, *Phys. Rev. Mater.* **2**, 073404 (2018).
- ⁸¹J. Kim, H.-Y. Kim, J. H. Jeon, S. An, J. Hong, and J. Kim, *Appl. Surf. Sci.* **451**, 162–168 (2018).
- ⁸²M. Wang, M. Huang, D. Luo, Y. Li, M. Choe, W. K. Seong, M. Kim, S. Jin, M. Wang, S. Chatterjee, Y. Kwon, Z. Lee, and R. S. Ruoff, *Nature* **596**, 519–524 (2021).
- ⁸³E. N. Voloshina, Y. S. Dedkov, S. Torbrügge, A. Thissen, and M. Fonin, *Appl. Phys. Lett.* **100**, 241606 (2012).
- ⁸⁴S. Nie, N. C. Bartelt, J. M. Wofford, O. D. Dubon, K. F. McCarty, and K. Thürmer, *Phys. Rev. B* **85**, 205406 (2012).
- ⁸⁵G. Lippert, J. Dabrowski, M. Lemme, C. Marcus, O. Seifarth, and G. Lupina, *Phys. Status Solidi (B)* **248**, 2619–2622 (2011).
- ⁸⁶A. Chatterjee, M. Kruskopf, S. Wundrack, P. Hinze, K. Pierz, R. Stosch, and H. Scherer, *ACS Appl. Electron. Mater.* **4**, 5317–5325 (2022).
- ⁸⁷M. Suemitsu, S. Jiao, H. Fukidome, Y. Tateno, I. Makabe, and T. Nakabayashi, *J. Phys. D: Appl. Phys.* **47**, 094016 (2014).
- ⁸⁸N. Zebardastan, J. Bradford, J. Lipton-Duffin, J. MacLeod, K. K. Ostrikov, M. Tomellini, and N. Motta, *Nanotechnology* **34**, 105601 (2022).
- ⁸⁹C. H. Lui, L. Liu, K. F. Mak, G. W. Flynn, and T. F. Heinz, *Nature* **462**, 339–341 (2009).
- ⁹⁰G. Lippert, J. Dabrowski, Y. Yamamoto, F. Herziger, J. Maultzsch, M. C. Lemme, W. Mehr, and G. Lupina, *Carbon* **52**, 40–48 (2013).
- ⁹¹J. Sun, Y. Chen, M. K. Priyadarshi, Z. Chen, A. Bachmatiuk, Z. Zou, Z. Chen, X. Song, Y. Gao, M. H. Rummeli, Y. Zhang, and Z. Liu, *Nano Lett.* **15**, 5846–5854 (2015).
- ⁹²H. J. Song, M. Son, C. Park, H. Lim, M. P. Levendorf, A. W. Tsen, J. Park, and H. C. Choi, *Nanoscale* **4**, 3050 (2012).
- ⁹³Z. Chen, C. Xie, W. Wang, J. Zhao, B. Liu, J. Shan, X. Wang, M. Hong, L. Lin, L. Huang, X. Lin, S. Yang, X. Gao, Y. Zhang, P. Gao, K. S. Novoselov, J. Sun, and Z. Liu, *Sci. Adv.* **7**, eabk0115 (2021).
- ⁹⁴J. Park, J. Lee, J.-H. Choi, D. K. Hwang, and Y.-W. Song, *Sci. Rep.* **5**, 11839 (2015).
- ⁹⁵A. K. Geim and I. V. Grigorieva, *Nature* **499**, 419–425 (2013).
- ⁹⁶K. Chung, C.-H. Lee, and G.-C. Yi, *Science* **330**, 655–657 (2010).
- ⁹⁷J. Kim, C. Bayram, H. Park, C.-W. Cheng, C. Dimitrakopoulos, J. A. Ott, K. B. Reuter, S. W. Bedell, and D. K. Sadana, *Nat. Commun.* **5**, 4836 (2014).
- ⁹⁸Y. Kim, S. S. Cruz, K. Lee, B. O. Alawode, C. Choi, Y. Song, J. M. Johnson, C. Heideberger, W. Kong, S. Choi, K. Qiao, I. Almansouri, E. A. Fitzgerald, J. Kong, A. M. Kolpak, J. Hwang, and J. Kim, *Nature* **544**, 340–343 (2017).
- ⁹⁹Z. Lu, L. Zhang, X. Wen, A. Jog, K. Kisslinger, L. Gao, J. Shi, D. Gall, M. A. Washington, G.-C. Wang, and T.-M. Lu, *ACS Appl. Electron. Mater.* **4**, 5775–5788 (2022).
- ¹⁰⁰X. Huang, J. Guan, Z. Lin, B. Liu, S. Xing, W. Wang, and J. Guo, *Nano Lett.* **17**, 4619–4623 (2017).
- ¹⁰¹S. Grimme, *J. Comput. Chem.* **27**, 1787–1799 (2006).
- ¹⁰²S. Grimme, J. Antony, S. Ehrlich, and H. Krieg, *J. Chem. Phys.* **132**, 154104 (2010).
- ¹⁰³J. Klimeš, D. R. Bowler, and A. Michaelides, *J. Phys.: Condens. Matter* **22**, 022201 (2010).
- ¹⁰⁴J. Klimeš, D. R. Bowler, and A. Michaelides, *Phys. Rev. B* **83**, 195131 (2011).
- ¹⁰⁵M. Gao, Y. Pan, L. Huang, H. Hu, L. Z. Zhang, H. M. Guo, S. X. Du, and H.-J. Gao, *Appl. Phys. Lett.* **98**, 033101 (2011).
- ¹⁰⁶M. Gao, Y. Pan, C. Zhang, H. Hu, R. Yang, H. Lu, J. Cai, S. Du, F. Liu, and H.-J. Gao, *Appl. Phys. Lett.* **96**, 053109 (2010).
- ¹⁰⁷H. W. Kim, W. Ko, J. Ku, Y. Kim, S. Park, and S. Hwang, *J. Phys. Chem. C* **121**, 25074–25078 (2017).
- ¹⁰⁸G. Kresse and J. Furthmüller, *Comput. Mater. Sci.* **6**, 15–50 (1996).
- ¹⁰⁹J. P. Perdew, K. Burke, and M. Ernzerhof, *Phys. Rev. Lett.* **77**, 3865–3868 (1996).
- ¹¹⁰H. Kang, P. Tang, H. Shu, Y. Zhang, Y. Liang, J. Li, Z. Chen, Y. Sui, S. Hu, S. Wang, S. Zhao, X. Zhang, C. Jiang, Y. Chen, Z. Xue, M. Zhang, D. Jiang, G. Yu, S. Peng, Z. Jin, and X. Liu, *Carbon* **181**, 225–233 (2021).
- ¹¹¹Y. Li, D. Subramaniam, N. Atodiresi, P. Lazić, V. Caciuc, C. Pauly, A. Georgi, C. Busse, M. Liebmann, S. Blügel, M. Prutzer, M. Morgenstern, and R. Mazzarello, *Adv. Mater.* **25**, 1967–1972 (2013).
- ¹¹²H. Chen, Y. Que, L. Tao, Y.-Y. Zhang, X. Lin, W. Xiao, D. Wang, S. Du, S. T. Pantelides, and H. J. Gao, *Nano Res.* **11**, 3722–3729 (2018).
- ¹¹³H.-B. Li, A. J. Page, C. Hettich, B. Aradi, C. Köhler, T. Frauenheim, S. Irle, and K. Morokuma, *Chem. Sci.* **5**, 3493–3500 (2014).
- ¹¹⁴B.-W. Li, D. Luo, L. Zhu, X. Zhang, S. Jin, M. Huang, F. Ding, and R. S. Ruoff, *Adv. Mater.* **30**, 1706504 (2018).
- ¹¹⁵M. A. Bissett, S. Konabe, S. Okada, M. Tsuji, and H. Ago, *ACS Nano* **7**, 10335–10343 (2013).
- ¹¹⁶C. C. Silva, M. Iannuzzi, D. A. Duncan, P. T. Ryan, K. T. Clarke, J. T. Kühle, J. Cai, W. Jolie, C. Schlueter, T. L. Lee, and C. Busse, *J. Phys. Chem. C* **122**, 18554–18561 (2018).
- ¹¹⁷D. Martocchia, P. R. Willmott, T. Brugger, M. Björck, S. Günther, C. M. Schlepütz, A. Cervellino, S. A. Pauli, B. D. Patterson, S. Marchini, J. Wintterlin, W. Moritz, and T. Greber, *Phys. Rev. Lett.* **101**, 126102 (2008).
- ¹¹⁸L. Gao, Y. Liu, T. Ma, R. Shi, Y. Hu, and J. Luo, *Appl. Phys. Lett.* **108**, 261601 (2016).
- ¹¹⁹L. Zhu and F. Ding, *Nanoscale Horiz.* **4**, 625–633 (2019).
- ¹²⁰J. Lu, P. S. E. Yeo, C. K. Gan, P. Wu, and K. P. Loh, *Nat. Nanotechnol.* **6**, 247–252 (2011).
- ¹²¹J. M. Soler, E. Artacho, J. D. Gale, A. García, J. Junquera, P. Ordejón, and D. Sánchez-Portal, *J. Phys.: Condens. Matter* **14**, 2745–2779 (2002).
- ¹²²P. Giannozzi, O. Andreussi, T. Brumme, O. Bunau, M. B. Nardelli, M. Calandra, R. Car, C. Cavazzoni, D. Ceresoli, M. Cococcioni, N. Colonna, I. Carnimeo, A. Dal Corso, S. de Gironcoli, P. Delugas, R. A. DiStasio Jr., A. Ferretti, A. Floris, G. Fratesi, G. Fugallo, R. Gebauer, U. Gerstmann, F. Giustino, T. Gorni, J. Jia, M. Kawamura, H.-Y. Ko, A. Kokalj, E. Küçükbenli, M. Lazzeri, M. Marsili, N. Marzari, F. Mauri, N. L. Nguyen, H.-V. Nguyen, A. Otero-de-la-Roza, L. Paulatto, S. Poncè, D. Rocca, R. Sabatini, B. Santra, M. Schlipf, A. P. Seitsonen, A. Smogunov, I. Timrov, T. Thonhauser, P. Umari, N. Vast, X. Wu, and S. Baroni, *J. Phys.: Condens. Matter* **29**, 465901 (2017).
- ¹²³T. Wu, X. Zhang, Q. Yuan, J. Xue, G. Lu, Z. Liu, H. Wang, H. Wang, F. Ding, Q. Yu, X. Xie, and M. Jiang, *Nat. Mater.* **15**, 43–47 (2016).
- ¹²⁴K. Yu, W. Zhao, X. Wu, J. Zhuang, X. Hu, Q. Zhang, J. Sun, T. Xu, Y. Chai, F. Ding, and L. Sun, *Nano Res.* **11**, 2809–2820 (2018).
- ¹²⁵G. te Velde, F. M. Bickelhaupt, E. J. Baerends, C. Fonseca Guerra, S. J. A. van Gisbergen, J. G. Snijders, and T. Ziegler, *J. Comput. Chem.* **22**, 931–967 (2001).
- ¹²⁶W. Zhang and A. C. T. van Duin, *Chem. Mater.* **32**, 8306–8317 (2020).
- ¹²⁷J. Gao, J. Yip, J. Zhao, B. I. Yakobson, and F. Ding, *J. Am. Chem. Soc.* **133**, 5009–5015 (2011).
- ¹²⁸R. C. Longo, H. Ueda, K. Cho, A. Ranjan, and P. L. G. Ventzek, *ACS Appl. Mater. Interfaces* **14**, 9492–9503 (2022).
- ¹²⁹Y. Xie, T. Cheng, C. Liu, K. Chen, Y. Cheng, Z. Chen, L. Qiu, G. Cui, Y. Yu, L. Cui, M. Zhang, J. Zhang, F. Ding, K. Liu, and Z. Liu, *ACS Nano* **13**, 10272–10278 (2019).
- ¹³⁰Q. Chen, K. Yang, B. Shi, X. Yi, J. Wang, J. Li, and Z. Liu, *Adv. Mater.* **35**, 2211075 (2023).
- ¹³¹G. D. Förster, F. Rabilloud, and F. Calvo, *Phys. Rev. B* **92**, 165425 (2015).
- ¹³²H.-H. Chen, S. H. Su, S.-L. Chang, B.-Y. Cheng, C.-W. Chong, J. C. A. Huang, and M.-F. Lin, *Carbon* **93**, 180–186 (2015).
- ¹³³B. Li, J. Yin, X. Liu, H. Wu, J. Li, X. Li, and W. Guo, *Nat. Nanotechnol.* **14**, 567–572 (2019).
- ¹³⁴Z. Wang, D.-K. Ki, H. Chen, H. Berger, A. H. MacDonald, and A. F. Morpurgo, *Nat. Commun.* **6**, 8339 (2015).

- ¹³⁵S. Wu, S. Buckley, J. R. Schaibley, L. Feng, J. Yan, D. G. Mandrus, F. Hatami, W. Yao, J. Vuckovic, A. Majumdar, and X. Xu, *Nature* **520**, 69–72 (2015).
- ¹³⁶Z. Lin, B. R. Carvalho, E. Kahn, R. Lv, R. Rao, H. Terrones, M. A. Pimenta, and M. Terrones, *2D Mater.* **3**, 022002 (2016).
- ¹³⁷N. Mounet, M. Gibertini, P. Schwaller, D. Campi, A. Merkys, A. Marrazzo, T. Sohier, I. E. Castelli, A. Cepellotti, G. Pizzi, and N. Marzari, *Nat. Nanotechnol.* **13**, 246–252 (2018).
- ¹³⁸H. Yin, Z. Sun, Z. Wang, D. Tang, C. H. Pang, X. Yu, A. S. Barnard, H. Zhao, and Z. Yin, *Cell Rep. Phys. Sci.* **2**, 100482 (2021).
- ¹³⁹A. C. Rajan, A. Mishra, S. Satsangi, R. Vaish, H. Mizuseki, K.-R. Lee, and A. K. Singh, *Chem. Mater.* **30**, 4031–4038 (2018).
- ¹⁴⁰A. Y.-T. Wang, R. J. Murdock, S. K. Kauwe, A. O. Oliynyk, A. Gurlo, J. Brgoch, K. A. Persson, and T. D. Sparks, *Chem. Mater.* **32**, 4954–4965 (2020).
- ¹⁴¹Y. Liu, T. Zhao, W. Ju, and S. Shi, *J. Materiomics* **3**, 159–177 (2017).
- ¹⁴²B. Ryu, L. Wang, H. Pu, M. K. Y. Chan, and J. Chen, *Chem. Soc. Rev.* **51**, 1899–1925 (2022).
- ¹⁴³N. Yoshihara, Y. Tahara, and M. Noda, “Machine learning method for determining chemical vapor deposition conditions for large-area graphene growth,” *Asia-Pac. J. Chem. Eng.* (published online).
- ¹⁴⁴Y. Du, Z. Yin, J. Zhu, X. Huang, X.-J. Wu, Z. Zeng, Q. Yan, and H. Zhang, *Nat. Commun.* **3**, 1177 (2012).
- ¹⁴⁵B. Anasori, M. R. Lukatskaya, and Y. Gogotsi, *Nat. Rev. Mater.* **2**, 16098 (2017).
- ¹⁴⁶P. Rowe, G. Csányi, D. Alfe, and A. Michaelides, *Phys. Rev. B* **97**, 054303 (2018).
- ¹⁴⁷V. L. Deringer, N. Bernstein, G. Csányi, C. Ben Mahmoud, M. Ceriotti, M. Wilson, D. A. Drabold, and S. R. Elliott, *Nature* **589**, 59–64 (2021).